Two-Dimensional Analysis of Rotor Suction and the Impact on Rotor-Stator Interaction Noise

by

Belva J. Hayden

B.S. Aerospace Engineering
University of Cincinnati (Cincinnati, OH), 1989

SUBMITTED TO THE DEPARTMENT OF
AERONAUTICS AND ASTRONAUTICS IN PARTIAL
FULFILLMENT OF THE REQUIREMENTS FOR THE
DEGREE OF

MASTER OF SCIENCE IN AERONAUTICS AND ASTRONAUTICS

at the

MASSACHUSETTS INSTITUTE OF TECHNOLOGY

September 1994

Signature of Author _____

Department of Aeronautics and Astronautics
August 19, 1994

Certified by _____

Professor Ian A. Waitz
Thesis Supervisor

Accepted by _____

Professor Harold Y. Wachman
Chairman, Department Graduate Committee

MASSACHUSETTS INSTITUTE

SEP 21 1994

Aero

Two-Dimensional Analysis of Rotor Suction and the Impact on Rotor-Stator Interaction Noise

by

Belva J. Hayden

Submitted to the Department of Aeronautics and Astronautics
on August 19, 1995 in partial fulfillment of the
requirements for the degree of Master of Science in
Aeronautics and Astronautics

Abstract

Fan rotor/stator interaction noise is expected to be a dominant noise source for next generation gas turbine engines. A new method of reducing fan noise which uses boundary layer suction on the rotor to reduce the rotor wake was examined. Two-dimensional, numerical simulations of two fan geometries were used to determine the impact of rotor boundary layer suction on stator unsteady loading. Suction was implemented on the suction surface of the rotor blade only. Wake reduction was limited by the trailing edge thickness of the rotor blade and the contribution of the boundary layer on the pressure surface of the blade. The maximum reduction of unsteady stator loading was approximately 25%, and was due primarily to the reduction in velocity deficit with suction.

Thesis Supervisor: Dr. Ian A. Waitz

Title: Assistant Professor of Aeronautics and Astronautics

Table of Contents

List of Figures

5

List of Tables

9

Nomenclature

c   blade chord

C_d profile drag coefficient

C_l lift coefficient

d   blade pitch

G   coefficient of non-steady upwash

h   shape parameter

h_k kinematic shape parameter

K   dimensionless half-width of viscous wake

K_n modified Bessel function of the second kind

L(t)   unsteady lift force

M   Mach number

Re   Reynold's Number

S(ω)   Sear's function

t   time

t_{TE} trailing edge thickness of blade

u   perturbation velocity

U	freestream velocity
u_c	Wake centerline velocity deficit
v	velocity
Y	half-width of wake

Symbols

δ	boundary layer thickness
δ^*	displacement thickness
θ	momentum thickness
ν	circular frequency
ω	reduced frequency $(2\pi/\nu)$
ρ	gas density

Chapter 1

1.0 Introduction

Community noise reduction has become a major consideration in subsonic transport engine design. In the 1960's, when the industry moved to high bypass ratio turbofan engines to increase efficiency, reduced noise was an added benefit. Since that time, however, there have been only evolutionary advances in methods to reduce aircraft noise. As regulatory standards for community noise continue to tighten, engine manufacturers are being challenged to design quieter, higher thrust engines with increased efficiency and reduced emissions. Current noise reduction technology is insufficient to meet anticipated community noise requirements over the next decade.

Rotor/stator interaction noise is expected to be a dominant noise source on next generation gas turbine engines. The objective of this research is to examine a new method of reducing fan rotor/stator interaction noise. The method centers on the use of boundary layer suction along the rotor chord to reduce the magnitude of the rotor wake and thereby reduce unsteady loading on the stator. Results from two-dimensional computational models are presented to describe the impact of boundary layer suction on the rotor wake and the unsteady loading the rotor wake produces on the stator.

Fan rotor/stator interaction noise results when wakes shed from the rotor cause unsteady loading on the stator. For subsonic relative blade velocities, Kantola and Gliebe [Ref. 1] reported that the unsteady stator loading is the primary noise source for high bypass ratio engines. A simplified model of rotor/stator interaction was presented by Kemp and Sears [Ref. 2, 3, 4] using a correlation of empirical data on airfoil wake behavior presented by Silverstein [Ref. 5]. The Kemp and Sears model treats the stator blades as isolated thin airfoils. More detailed physical models have been developed by Amiet [Ref. 6] who included effects of compressibility, Goldstein and Atassi [Ref. 7] who included second order effects such as camber, thickness, and angle of attack in the analysis of unsteady flow on an airfoil due to a periodic gust, and Namba [Ref. 8] who presented a three-dimensional, compressible cascade analysis. The computational analysis used in this thesis includes cascade and compressibility effects and some comparisons are made to the wake model developed by Silverstein and the incompressible cascade model developed by Kemp and Sears.

It must be noted that all of the above models approximate the rotor wake as a steady velocity deficit in the rotor frame. However, Epstein et al. [Ref.. 9] have presented laser anemometer measurements from a compressor showing the significance of the unsteadiness in the wake. This unsteadiness may be an important contributor to broad band noise. The computational models used in this thesis limit consideration to time-averaged rotor wake characteristics.

Groeneweg [Ref. 10] describes several methods for reducing fan noise. These methods include adding fan duct acoustic treatments to absorb the noise, designing rotor blades with minimum blade section drag at operating conditions where noise levels are

13

critical, designing fans with rotor-stator spacing large enough for the rotor wakes to decay and mix before impinging on the stator blades, increasing the number of rotor wakes, and increasing stator chord to reduce the unsteady lift response. These methods are employed in current technology engines and are insufficient to meet the goal of 6EPNdB noise reduction recently established in the NASA Advanced Subsonic Technology Program for next-generation gas turbine engine technology.

A new approach for fan noise reduction has been proposed by Waitz [Ref. 11]. It is based on adding and/or removing fluid to modify the rotor wake and thus change the unsteady loading on the stator. The basic premises are that boundary layer suction on the rotor will reduce the width and depth of the wake, and that blowing from the trailing edge of the rotor will add momentum to the wake, thereby reducing the velocity defect. These techniques may also favorably impact unsteady (in the rotor frame) characteristics of the wake affecting broad band noise sources. An attractive aspect of this approach is that technology for designing and manufacturing blades with internal passages has been developed for turbine blades. Further, the Pratt and Whitney 4084 engine currently undergoing certification testing employs hollow fan blades as a means of achieving a weight reduction.

The research discussed herein focuses specifically on how suction of the rotor boundary layer impacts the rotor wake and the subsequent wake/stator interaction. The basis for the results presented is a two-dimensional computational model. For the applications of interest, the rotor/stator spacing is large enough that potential flow interaction effects between the rotor and stator can be neglected. This allowed the suction on the rotor and the impact on the stator to be considered in a two part analysis. The first

part involved a steady, viscous calculation on the rotor in the rotor reference frame. The second part of the analysis involved an unsteady, inviscid calculation on the stator using the wakes generated from the first part of the analysis as input. MISES [Ref. 12], a two-dimensional, steady, viscous cascade code was used to describe the rotor wake characteristics, both with and without suction. For the second part, a two-dimensional, unsteady, inviscid cascade code, UNSFLO [Ref. 13], was used to calculate unsteady loading on the stator due to the upstream rotor wakes.

Two fan geometries were investigated in this study: the NASA Low Aspect Ratio Fan (Stage 67) and a geometry representative of a modern high bypass ratio fan. Extensive experimental studies and computational analyses have been performed on the Stage 67 geometry (Strazizar [Ref. 14], Hathaway [Ref. 15], and Topol[Ref. 16]). The modern high bypass ratio fan geometry investigated will be the subject of future experiments in the MIT Blowdown Compressor. Midspan sections of both fans were used as a basis for the two-dimensional models discussed in this thesis.

The same parametric studies were done on each geometry and comparisons are discussed. Cases with suction on the rotor at 50%, 80% and 90% chord location, with 0%, 25%, 50%, and 75% of the boundary layer removed were examined at rotor-stator spacings of 2 and 3 rotor chordlengths. Boundary layer removal was implemented on the suction side of the rotor blade only.

Chapter 2 discusses the computational tools used to examine and model the rotor wakes and the resulting unsteady forces on the stator. Included in this discussion is a detailed description of the suction model incorporated into MISES. Chapter 3 describes the two geometries examined in this study. The results of the computational analyses are

discussed in Chapter 4. Finally, conclusions and recommendations are presented in

Chapter 5.

Chapter 2

2.0 Computational Model

For the applications of interest, the rotor-stator spacing is large enough that potential flow interaction effects between the rotor and stator can be neglected. Therefore, the suction on the rotor and the impact on the stator were considered in a two part analysis. The first part, a steady viscous calculation on the rotor, was performed using MISES [Ref. 12], a two-dimensional cascade code. The second part, an unsteady, inviscid calculation on the stator, was performed using UNSFLO [Ref. 13]. These computational models are described below.

2.1 MISES

MISES [Ref 12], a viscous, multiple blade, cascade code was modified to model suction, and then used to calculate boundary layer and wake characteristics. This code uses a Newton solution method to solve the steady two-dimensional Euler equations. Boundary layers and wakes are modeled and described with integral equations that are coupled with the inviscid flow (the grid for the inviscid flow region is displaced from the blade by the displacement thickness). Reference 12 includes a validation of the code with

comparisons of blade pressure distributions, displacement thickness, momentum thickness, and shape parameter calculations to experimental data. A complete description of how to use the code can be found in the User's Guide [Ref. 17].

MISES calculates the displacement thickness, momentum thickness, and kinematic shape parameter of the boundary layer along the rotor chord and in the wake. The transition point can either be calculated or specified and input manually. For the cases discussed in this thesis, transition was calculated by MISES. The velocity profile along the chord was calculated using a one-seventh profile in the turbulent region, and a Falkner-Skan profile in the laminar region. The wake boundary layer thickness was calculated assuming a cosine velocity profile. The wake characteristics are defined below.

The displacement thickness, δ^*, is related to the boundary layer thickness, δ, by

$$\delta^* = \frac{1-U_s}{2}\delta \ ,$$

where U_s is the velocity deficit in the wake defined by

$$1-U_s = \frac{4}{3}\frac{h_k-1}{h_k} \ .$$

where h_k is the kinematic shape parameter. The velocity profile in the wake was described using a cosine function valid only for $y \leq \delta$:

$$\frac{u}{u_e} = U_s + \frac{1-U_s}{2}\left(1-\cos\frac{\pi}{\delta}y\right).$$

An empirical wake correlation was developed by Topol [Ref. 16] from laser anemometer data described in Strazizar [Ref. 14]. A description of this correlation is found in Appendix B. The correlations were compared to the wake calculations made

using the MISES model for the baseline case where no suction was applied to the rotor. Figure 1 shows the wake momentum thickness versus axial position behind the Test Fan (described in Section 3.2) obtained using the rotor data correlation in Topol and the MISES calculations. Both models calculate comparable momentum thicknesses. (The Topol model shows a slight increase in momentum thickness with axial position, and thus does not conserve momentum as would be expected in the region of small axial pressure gradient downstream of the rotor in this particular geometry.)

The comparison with the empirical correlation presented by Topol was judged to be sufficient to support using MISES as a basis for modeling the wake in this study. The momentum thickness calculations from the Silverstein [Ref. 5] correlation (used in the analytical model developed by Kemp and Sears [Ref. 3]) did not compare as well. Figure 2 shows that momentum thickness grows significantly behind the airfoil and that momentum is not conserved as would be expected.
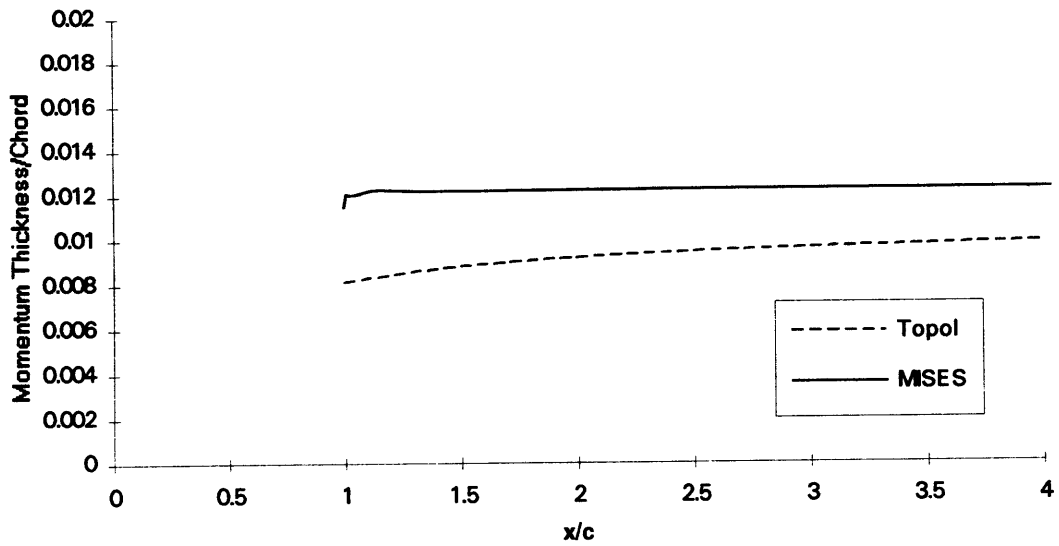
Figure 1. Momentum Thickness Comparison for MISES and Topol Wake Models.
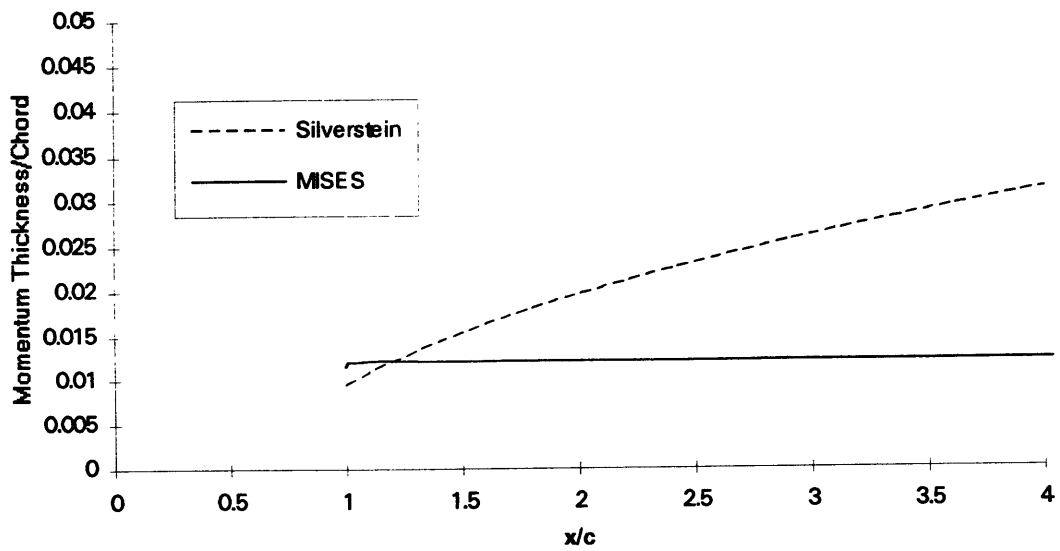
Figure 2. Momentum Thickness Comparison for MISES and Silverstein Wake Models.

2.1.1 General suction model in MISES.

The boundary layer equations in MISES were modified so that suction on the surface of the blade was modeled by removing a percentage of the momentum thickness and by changing the shape parameter and other boundary layer descriptors correspondingly. First, a one-seventh power boundary layer profile was assumed along the chord (all suction locations investigated were downstream of the boundary layer transition point). It was also assumed that the bottom of the boundary layer was removed due to the suction as shown in Figure 3, where the y' parameter corresponds to the portion of the boundary layer removed.

Figure 3. 1/7 Power Law Boundary Layer Profile.

To incorporate the suction model into MISES, a multiplier was used on the momentum thickness to simulate removal of the boundary layer. A correlation of the percentage drop in momentum thickness to shape parameter or displacement thickness was incorporated since all are dependent. This correlation was developed using the following boundary layer descriptors:
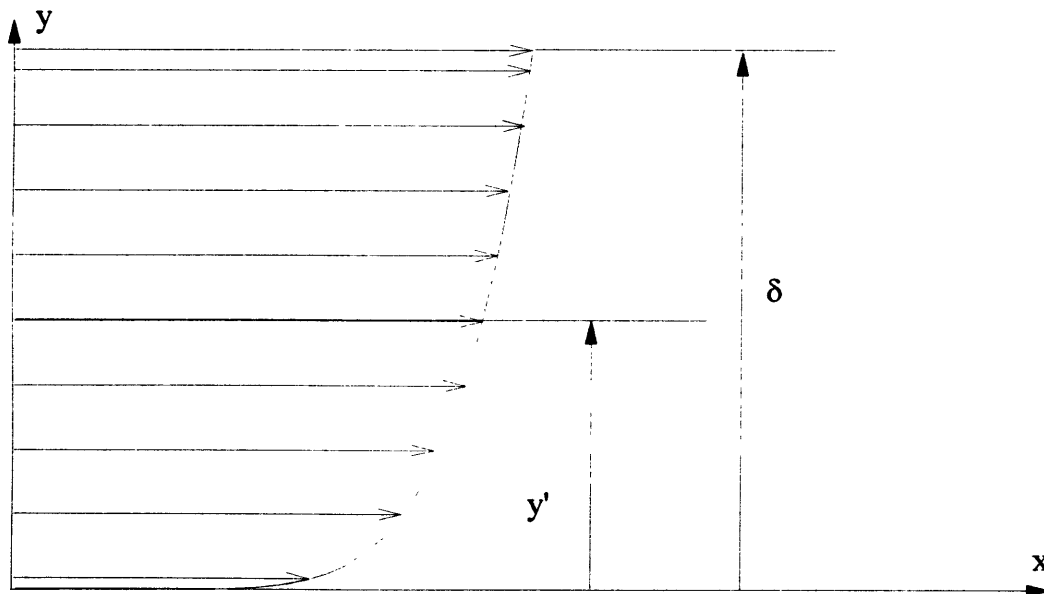
$$\theta = \int_0^\delta \frac{u}{U}\left(1 - \frac{u}{U}\right)dy \qquad \text{(momentum thickness)}$$

$$\delta^* = \int_0^\delta \left(1 - \frac{u}{U}\right)dy \qquad \text{(displacement thickness)}$$

$$h = \frac{\delta^*}{\theta} \qquad \text{(shape parameter)}$$

$$\frac{u}{U} = \left(\frac{y}{\delta}\right)^{1/7} \qquad \text{(velocity profile)}$$

Using the 1/7 velocity profile in the above equations results in

$$\theta = \frac{7}{72}\delta \,,$$

$$\delta^* = \frac{1}{8}\delta \,,$$

and

$$h = \frac{9}{7} \,.$$

After removing a percentage of the momentum thickness from the bottom of the boundary layer, the remaining momentum thickness is

$$\theta_{remaining} = \int_{y'}^{\delta} \frac{u}{U}\left(1 - \frac{u}{U}\right) dy .$$

For a 1/7 power law velocity profile, this may be written as

$$\frac{\theta_{remaining}}{\theta} = 1 + 8\left(\frac{y'}{\delta}\right)^{9/7} - 9\left(\frac{y'}{\delta}\right)^{8/7} .$$

Similarly, the remaining percentage of displacement thickness is

$$\frac{\delta_{remaining}}{\delta} = 1 - 8\frac{y'}{\delta} + 7\left(\frac{y'}{\delta}\right)^{8/7} , \text{ and}$$

the corresponding shape parameter fraction is

$$\frac{h_{remaining}}{h} = \frac{\delta^*_{remain}/\delta}{\theta_{remain}/\theta} .$$

Figure 4 shows the variation of δ^*, θ, and h as a function of y'/δ. Using this model, the shape parameter was scheduled to correspond with a given fraction of momentum thickness removed. The program was configured to spread the suction over a user specified number of cells to help reduce convergence errors. For the geometries examined in this thesis, suction was scheduled over two grid cells (approximately 2-3% chord).

Once the suction was calculated, the simulations were continued to the trailing edge and through the wake. The wake calculations were carried out approximately four to five chordlengths downstream of the rotor.
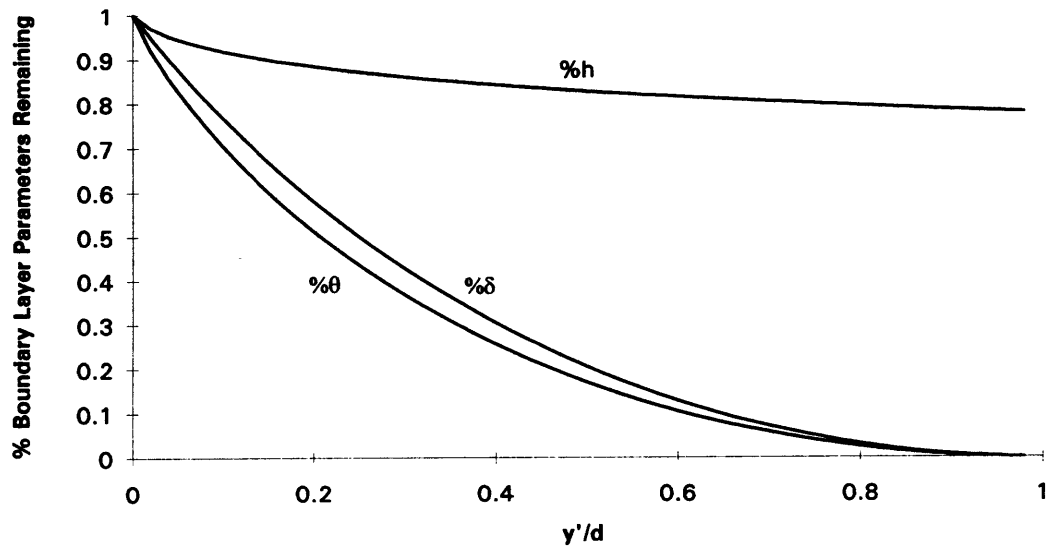
Figure 4. Variation of Boundary Layer Parameters With Suction for 1/7 Boundary Layer Profile.

2.2 UNSFLO

The unsteady loading calculations on the stator were performed using UNSFLO [Ref. 13]. UNSFLO is a computational code capable of solving two-dimensional inviscid or viscous, and steady or unsteady equations of motion on an unstructured grid. Quasi-three dimensional effects can also be included for a more representative model. UNSFLO employs a hybrid Euler/Navier-Stokes scheme, with the Euler algorithm used in the inviscid region and the Navier-Stokes algorithm used in the viscous region. UNSFLO also uses a time-inclined plane to allow the use of arbitrary wake-rotor, or rotor-stator, pitch ratios, such as was used for the cases presented in this thesis. A detailed description of the various modeling and numerical techniques used in UNSFLO is found in Giles [Ref. 13] and instructions on how to use the code are provided in the User's Guide [Ref. 18] The code has been validated by Manwaring and Wisler [Ref. 19].

The first step towards an unsteady solution using UNSFLO for a combined rotor wake/stator case was to generate a grid from the stator blade coordinates, the inlet and exit flow angles, and the pitch of the stator. A converged steady solution was then calculated on the stator grid using UNSFLO. Once this steady solution had converged, a file with multiple passages was created to allow UNSFLO to solve the unsteady problem with different rotor-stator pitch ratios. An unsteady solution was then calculated using the multiple-passage, steady flow file as the input flow file and the wake characteristics calculated in MISES as input parameters.

The input to UNSFLO accounted for the ratio of the stator blade pitch to the wake pitch and the angle of the wakes relative to the stator blades. UNSFLO has the option to model sinusoidal, Gaussian, or square wakes. A Gaussian profile was used for the cases

25

studied in this thesis. Wake profiles in the MISES code are described with a cosine

profile, but as shown in Figure 5, the cosine and Gaussian profiles used were nearly the

same. (The Gaussian profile yielded a 2-3% higher displacement thickness and

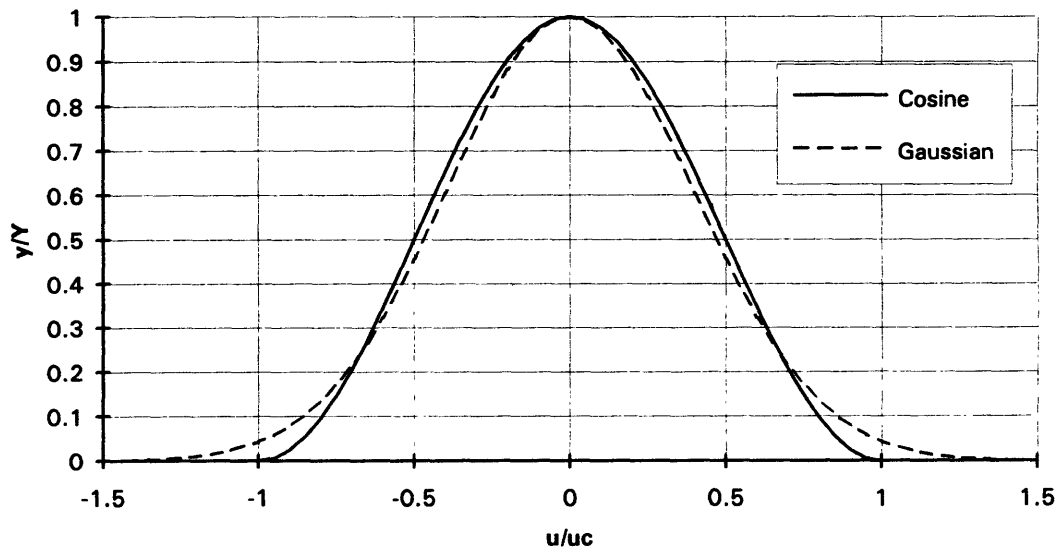momentum thickness.) UNSFLO also limits the wake width to no more than one rotor

pitch.

Figure 5. Comparison of Cosine and Gaussian Wake Profiles.

Chapter 3

3.0 Geometry

Two geometries were used in this study. The first is the NASA Stage 67 Fan, on which extensive computational and experimental work has been done. The second geometry is more typical of fan geometries for next-generation high bypass ratio turbofan engines. Details of each geometry are described below.

3.1 Stage 67

The first stage from the NASA low-aspect ratio fan (Stage 67) was used because a significant amount of experimental and computational work has been done on this stage, including wake measurements. Urasek [Ref. 20] presents detailed performance data at various operating conditions for a number of spanwise locations. These data were used to determine the proper conditions for the computational model. Table 1 summarizes Stage 67 fan characteristics. Since blade speeds are subsonic for the high bypass ratio fans, which are the primary focus of this research, a subsonic operating condition was chosen. The operating condition of 80% speed was used because it was a subsonic condition for the midspan section of the blade. The inlet Mach number was 0.806 and the rotor exit

Mach number was 0.525. An example of the rotor grid used in MISES is shown in Figure 7, and Figure 8 shows the stator grid used in the UNSFLO calculations.

Figure 6. Stage 67 First Stage Fan Geometry.

Table 1. Characteristics of Stage 1 of Stage 67 Fan.

	Rotor		Stator	
	Inlet	Exit	Inlet	Exit
Mach	0.806	0.525	0.5	0.452
Angle	57.3	36.2	37.6	01.6
Chord (m)	0.0933		0.0574	
Pitch (m)	0.0518		0.0335	
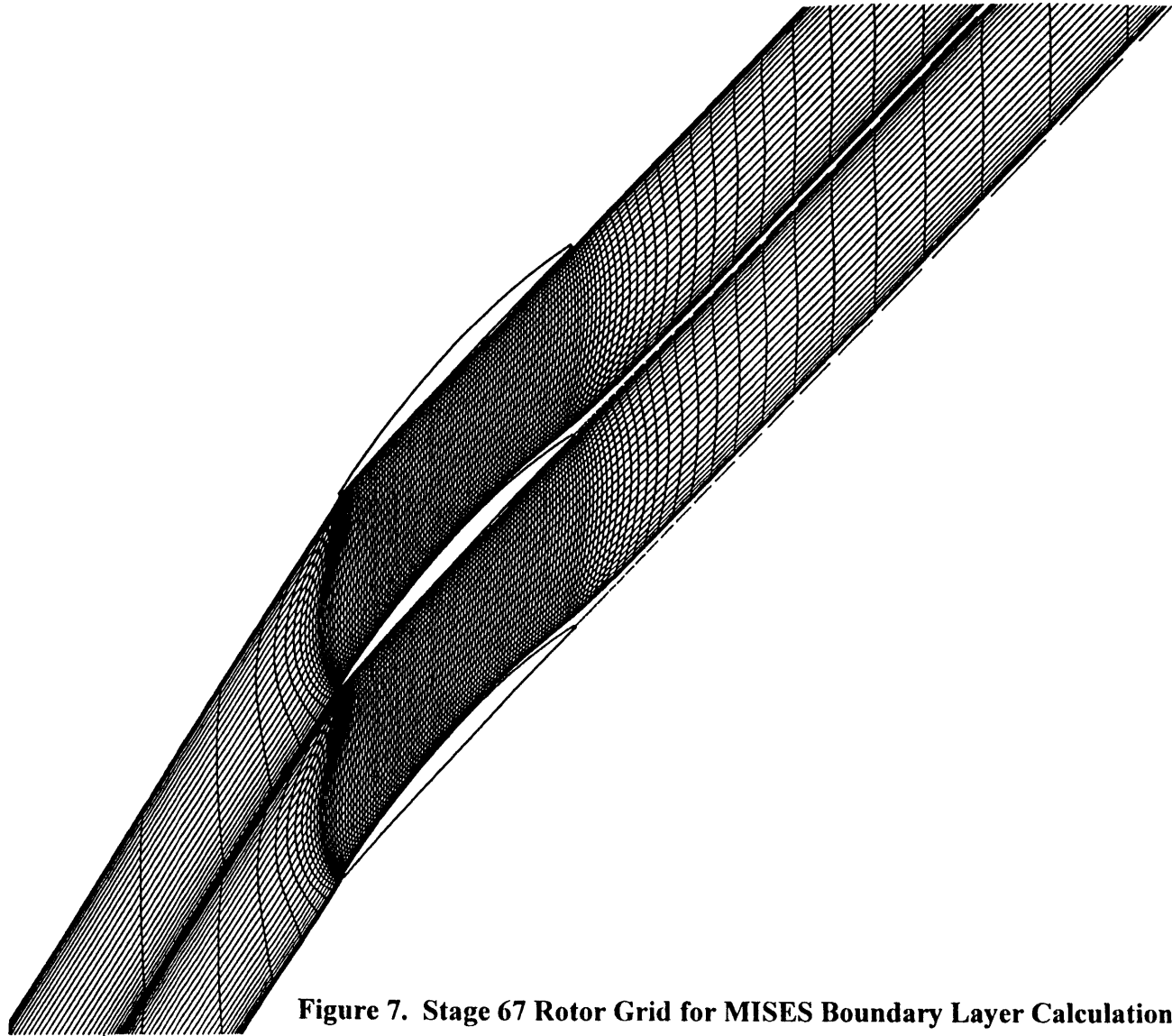
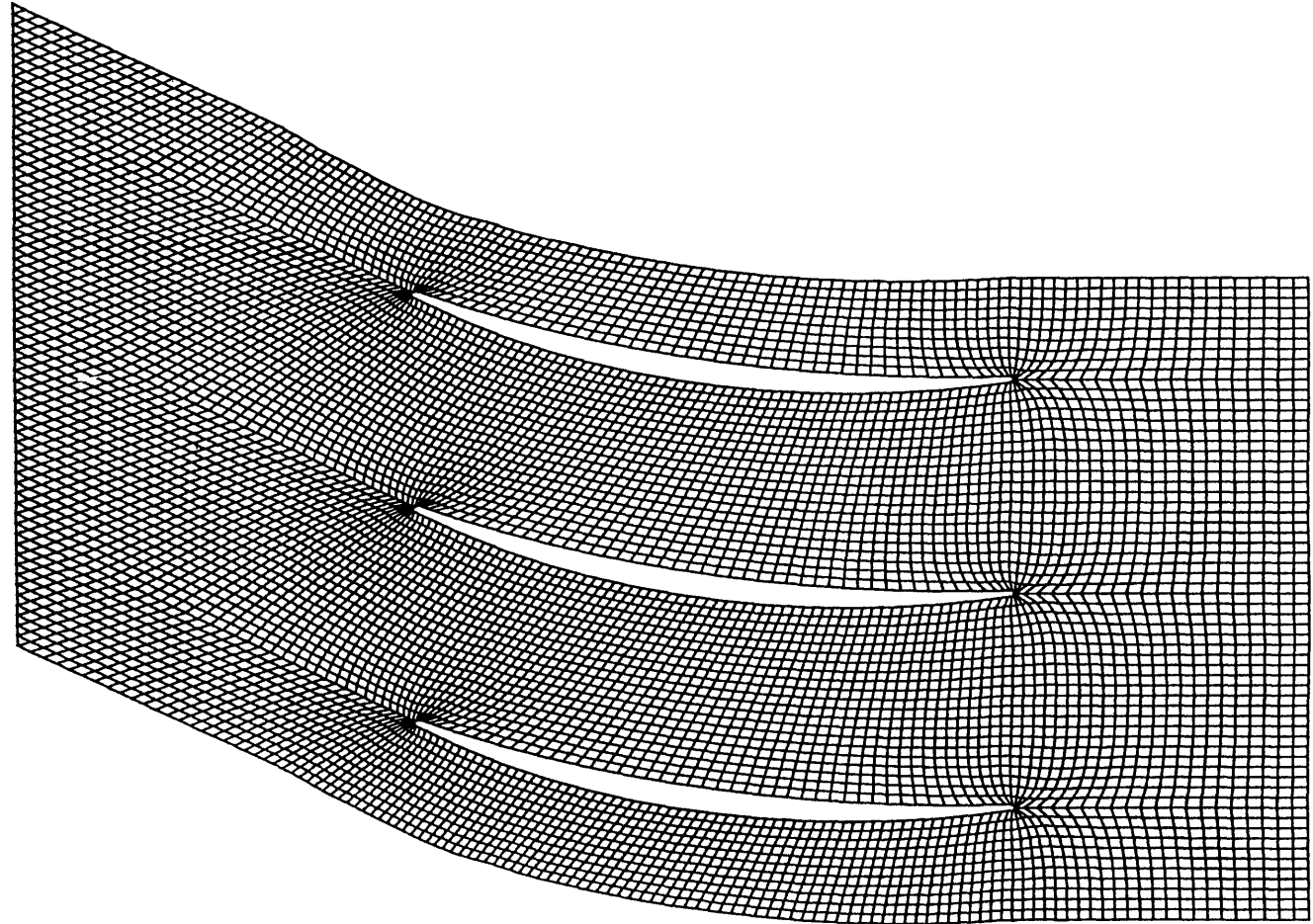Figure 7. Stage 67 Rotor Grid for MISES Boundary Layer Calculations.

Figure 8. Stage 67 Stator Grid for UNSFLO Unsteady Calculations.

3.2 Test Fan Geometry

A geometry similar to those used in modern high bypass ratio engines was also examined. The geometry was characterized by 40 rotor blades and 16 stator blades, with a rotor-stator spacing of approximately 2.5 rotor chordlengths. For the two-dimensional analysis, the midspan section of the model-scale, 22 inch diameter rotor stage shown in Figure 9 was used. This geometry will be used in future wake management experiments in the MIT Blowdown Compressor.

Table 2 summarizes the characteristics of the fan used in this study. Takeoff conditions were used. (It is during takeoff that fan noise has the most significant impact on the community.) The rotor inlet Mach number was 0.735 and the stator inlet Mach number was 0.526.

An example of the rotor grid used in MISES is shown in Figure 10, and Figure 11 shows the stator grid used in the UNSFLO calculations.

Figure 9. High Bypass Ratio Fan Geometry.

Table 2. High Bypass Ratio Fan Characteristics.

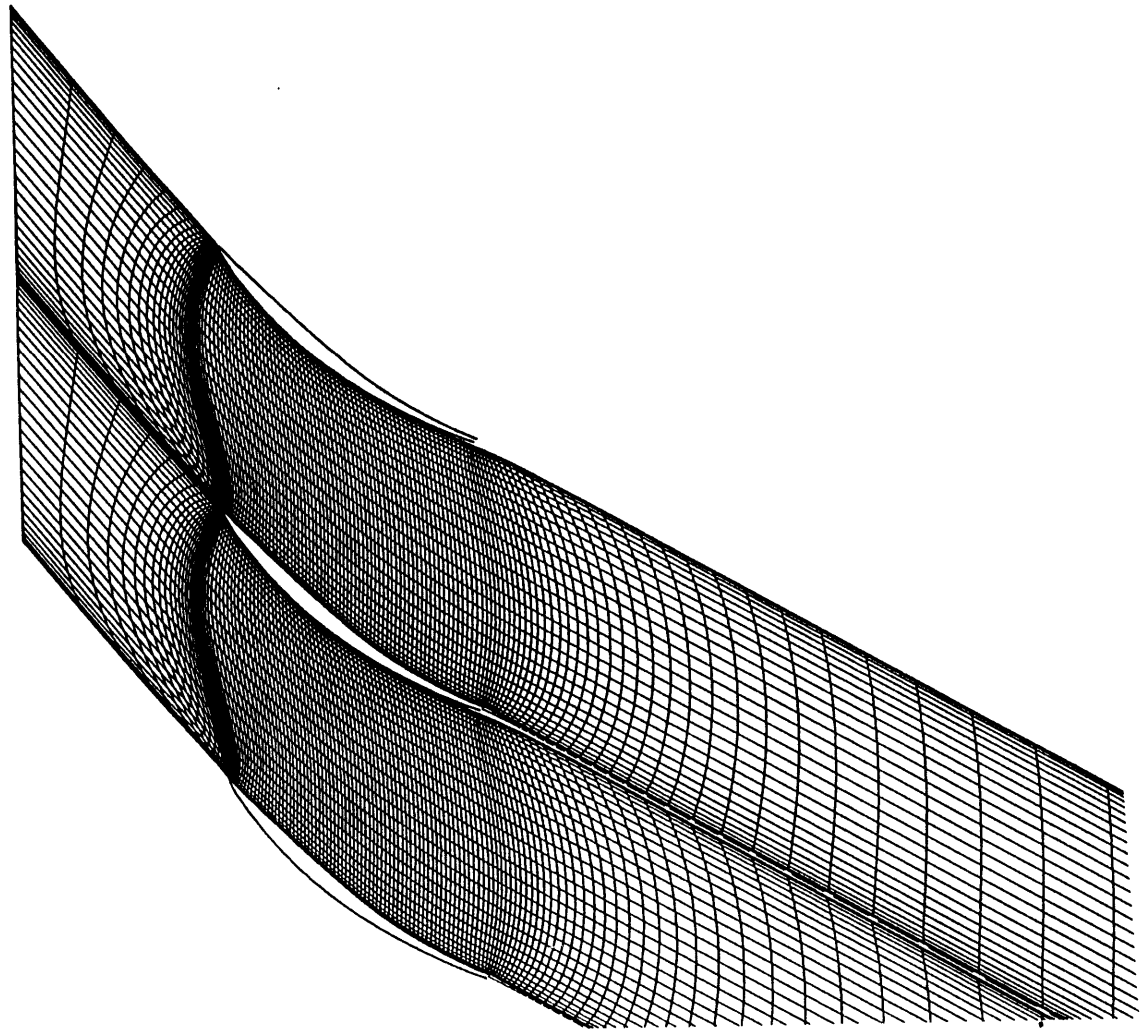|	Rotor		Stator	
	Inlet	Exit	Inlet	Exit
Mach	.735	.515	.526	.486
Angle	39.75°	58.9°	55.6°	89.75°
Chord (m)	.099		0.048	
Pitch (m)	.081		.052	

Figure 10. Test Fan Rotor Grid for MISES Boundary Layer Calculations.
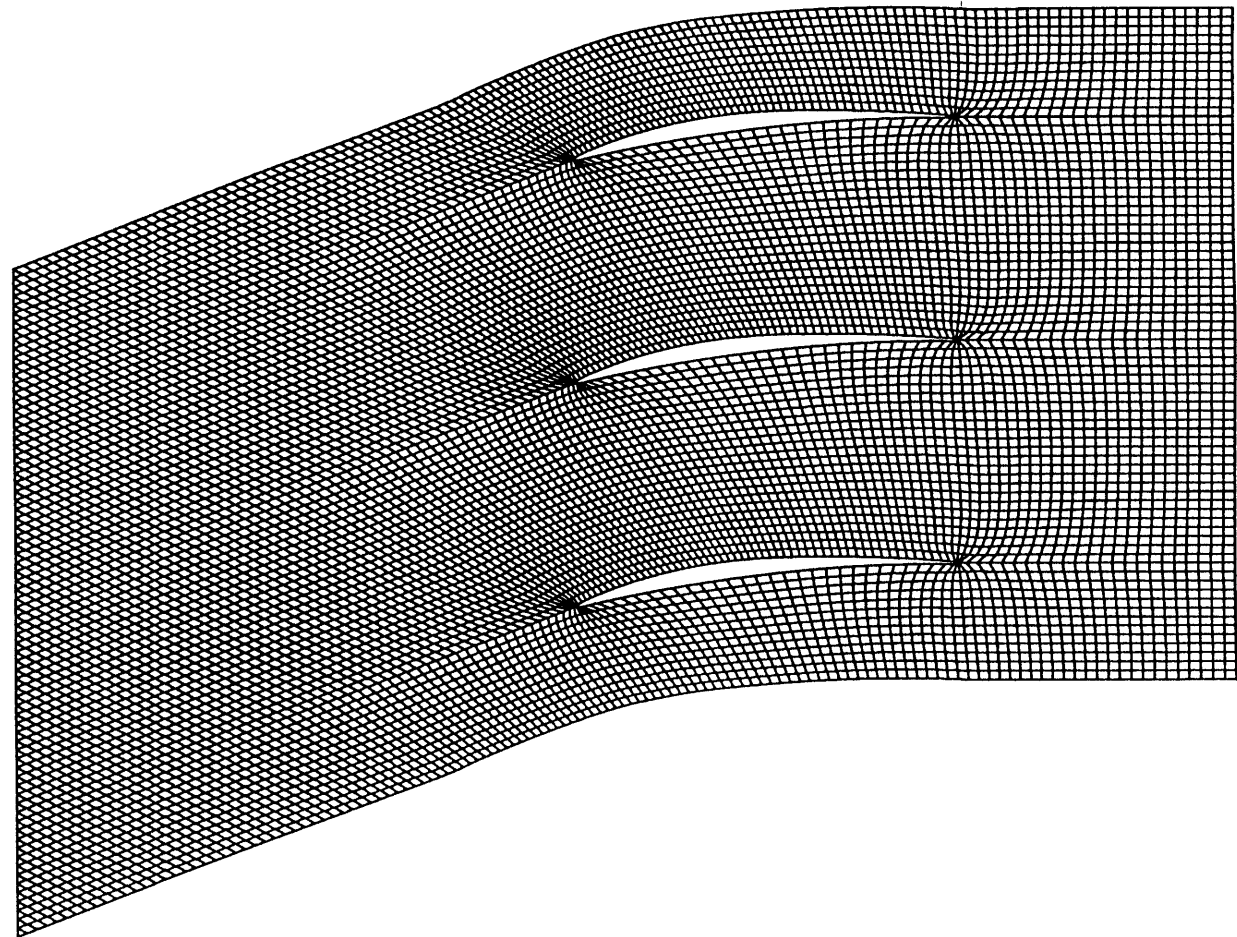
Figure 11. Test Fan Stator Grid for UNSFLO Unsteady Calculations.

Chapter 4

4.0 Results

Parametric studies of rotor suction configurations were completed on the two geometries described in Chapter 3. Suction of 25%, 50%, and 75% of the momentum thickness was examined at rotor locations of 50%, 80%, and 90% chord. Wake calculations were extended approximately four rotor chords downstream and wake data at two and three chordlengths downstream was used for unsteady loading calculations. A summary of baseline wake parameters and unsteady loading characteristics is presented in Section 4.1. Wake parameters and unsteady loading calculations for the two geometries with boundary layer suction applied are presented in Sections 4.2 and 4.3.

Unsteady loading results for the test fan geometry were also used to complete a study to determine the optimum placement of transducers to resolve unsteady loading on the stator blades in future experiments. This work is discussed in Section 4.4.

4.1 Baseline Performance with No Suction.

Figures 12 and 13 present displacement thickness and momentum thickness for the suction and pressure surfaces of the Stage 67 rotor blade for the case of no suction. These data show that the trailing edge thickness does not contribute significantly to the displacement thickness in the wake. (The trailing edge thickness was approximately 0.6% chord.) The results do show however, significant boundary layer growth near the trailing edge.

Figure 14 presents a contour plot of the perturbation velocity for the Stage 67 stator with no suction on the rotor for a rotor/stator axial spacing of two chordlengths. For this geometry the rotor/stator pitch ratio was 1.55, so approximately one to two wakes are present in each stator passage at a given instant in time. Figure 15 shows the unsteady loading on the stator for rotor/stator spacings of two and three chordlengths.

Similar data is shown in Figures 16-19 for the Test Fan geometry at baseline conditions. Figures 16 and 17 show examples of the displacement thickness and momentum thickness along the Test Fan rotor and into the wake. These figures show that the trailing edge thickness is responsible for approximately 50% of the wake displacement thickness. For this geometry the trailing edge thickness was approximately 1.3% chord.

The unsteady loading on the stator for rotor/stator spacings of two and three chordlengths is shown in Figure 18. Figure 19 presents a contour plot of the perturbation velocity for the Test Fan stator with no suction for a rotor/stator spacing of two chordlengths. The rotor/stator pitch ratio for the Test Fan (= 1.57) was similar to that for Stage 67, so again the wakes are fairly long wavelength disturbances with respect to the

stator chord. Figures 20 and 21 show the pressure profile for the case of no suction at different time steps. The perturbations are relatively small because of the large wake width and the small velocity deficit.
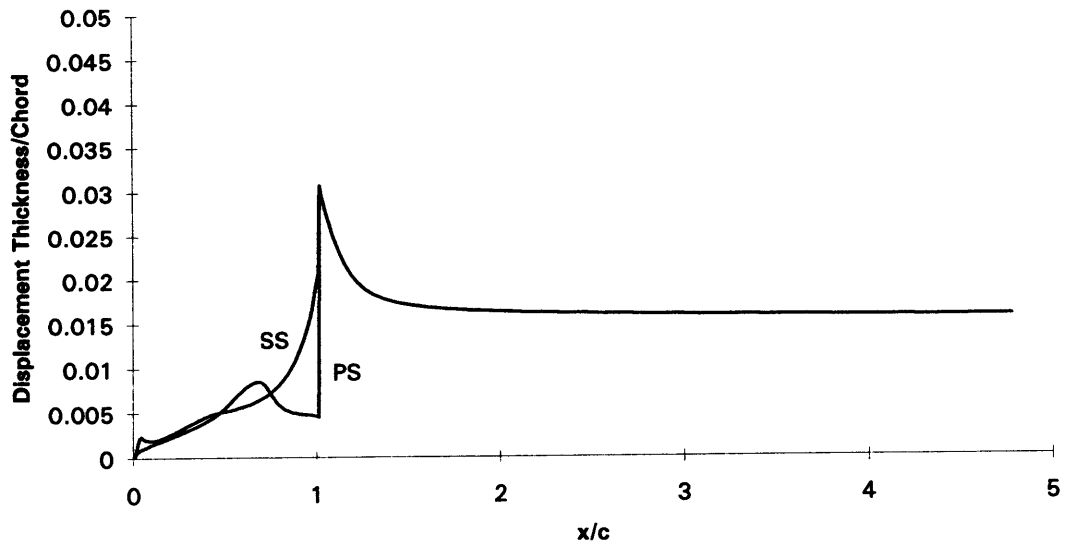
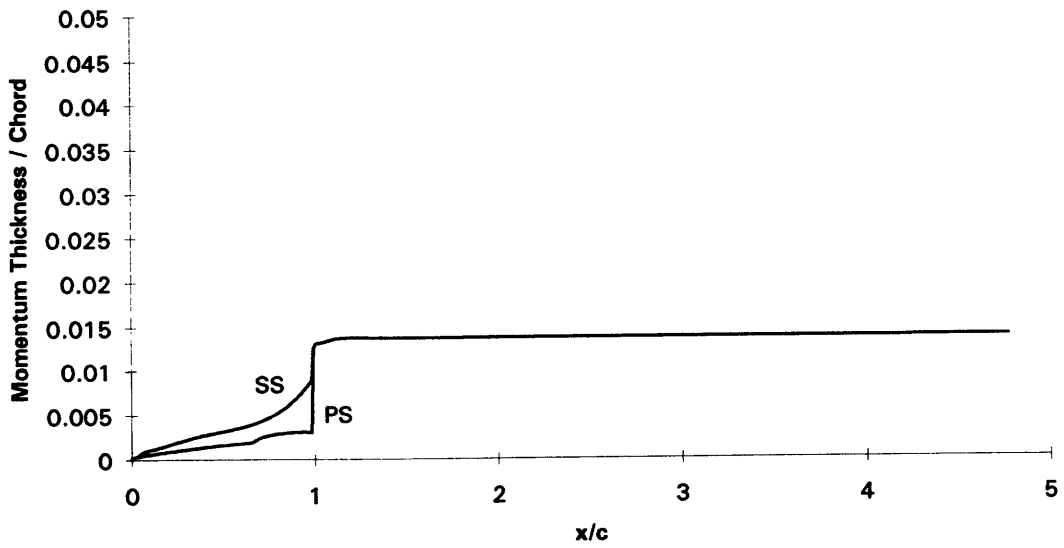**Figure 12. Stage 67 Rotor Displacement Thickness with No Suction.**

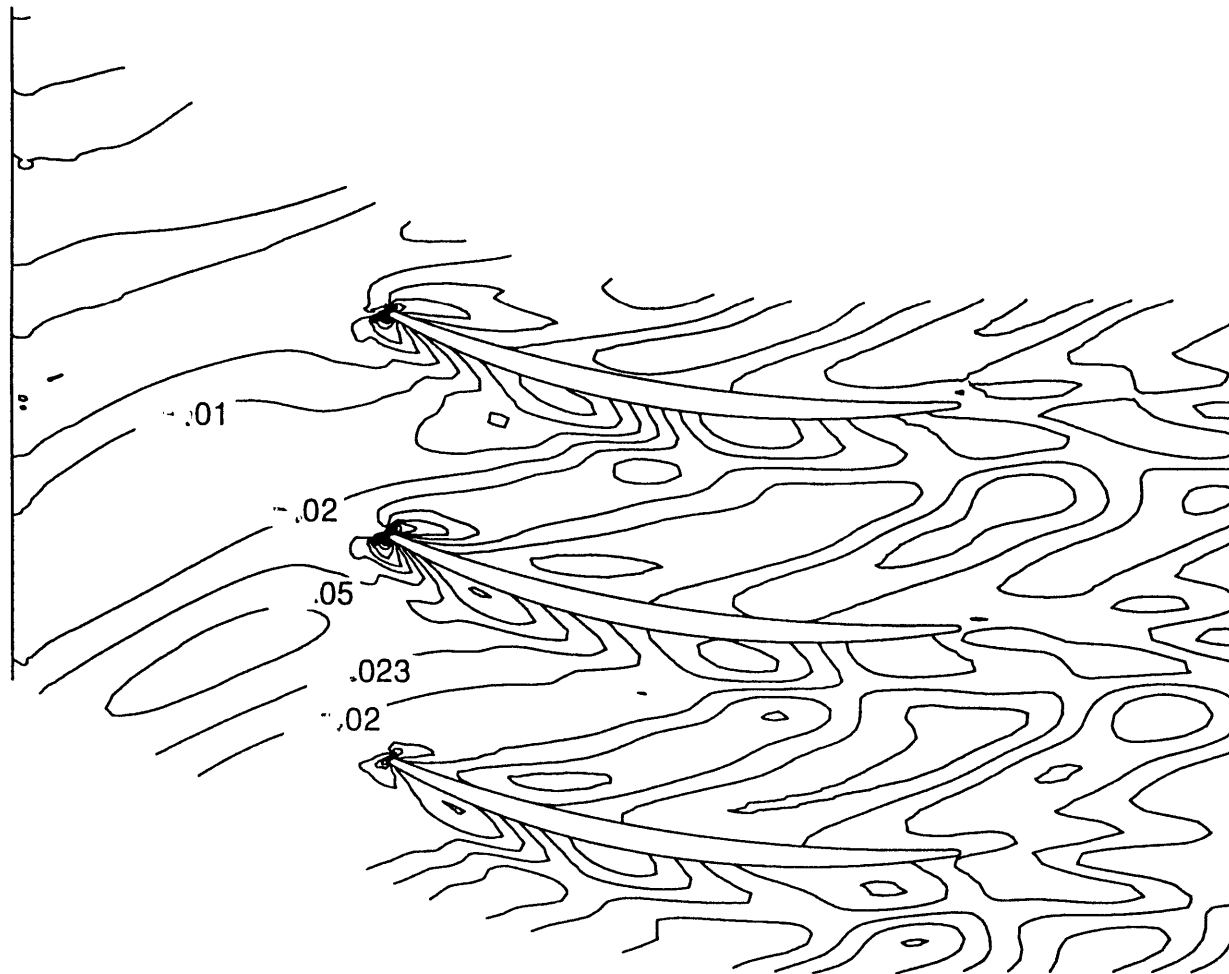**Figure 13. Stage 67 Rotor Momentum Thickness with No Suction.**

.01

-.02

.05

.023

-.02

Figure 14. Stage 67 Contour Plot of Perturbation Mach Number with No Suction (Wake Data at 2 Chordlengths Downstream of Rotor).
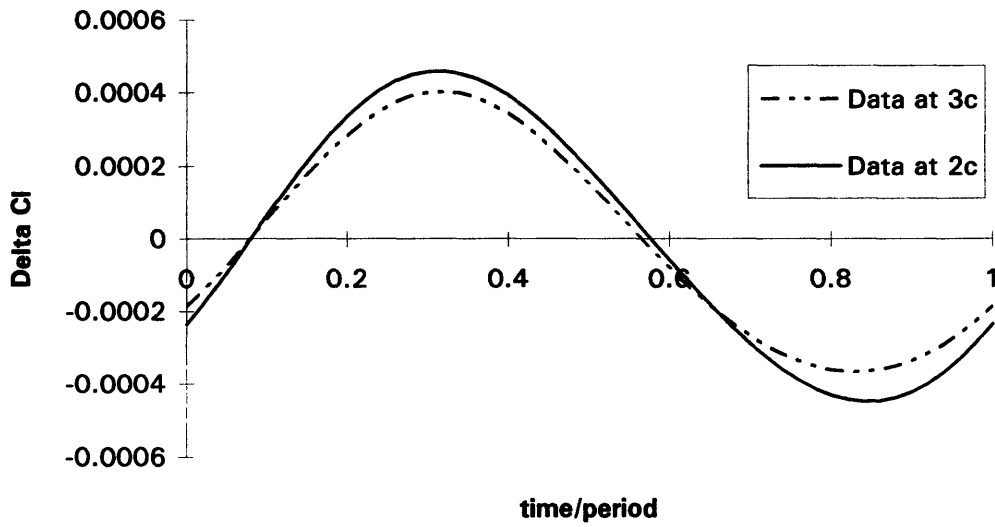
**Figure 15. Stage 67 Unsteady Loading on Stator, No Suction. (Wake Data at 2 and 3 Chordlengths Downstream of Rotor.)**
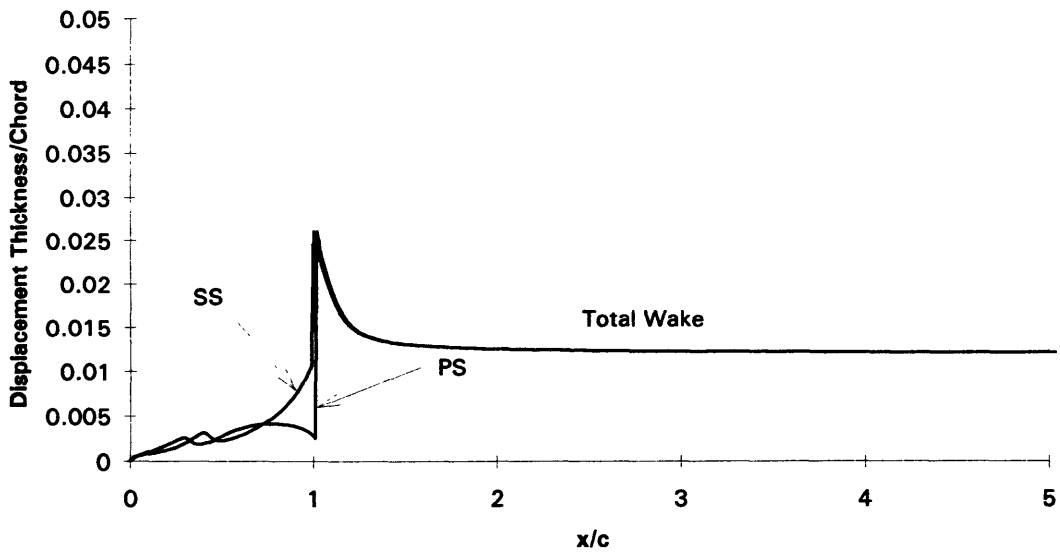
Figure 16. Test Fan Displacement Thickness with No Suction.
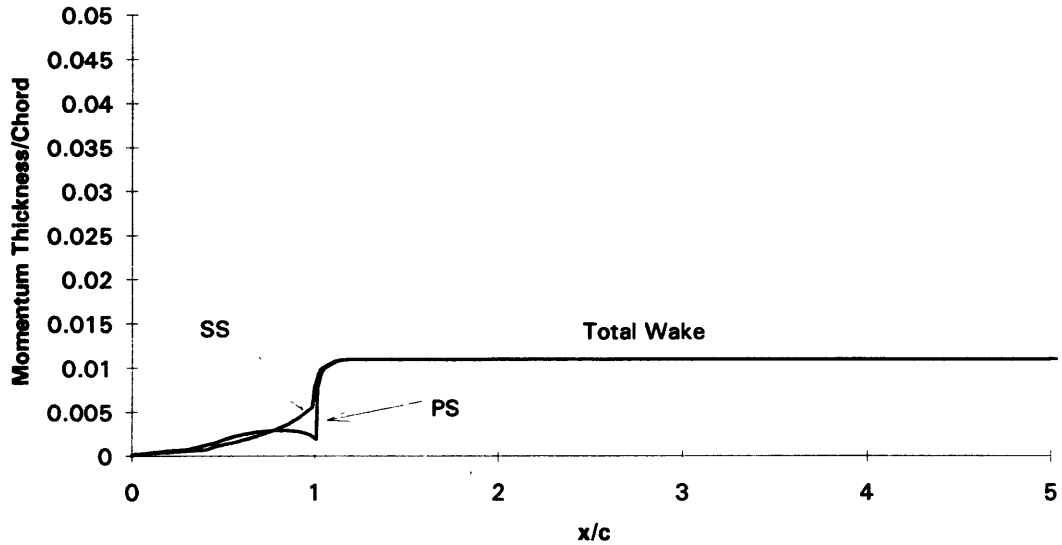
Figure 17. Test Fan Momentum Thickness with No Suction.
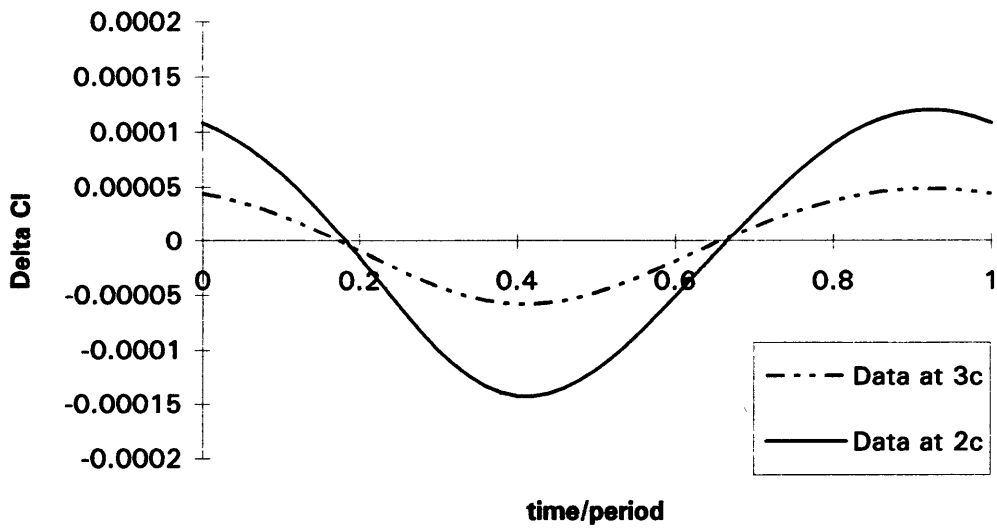
Figure 18. Test Fan Unsteady Loading on Stator, No Suction. (Wake Data at 2 and 3 Chordlengths Downstream of Rotor.)
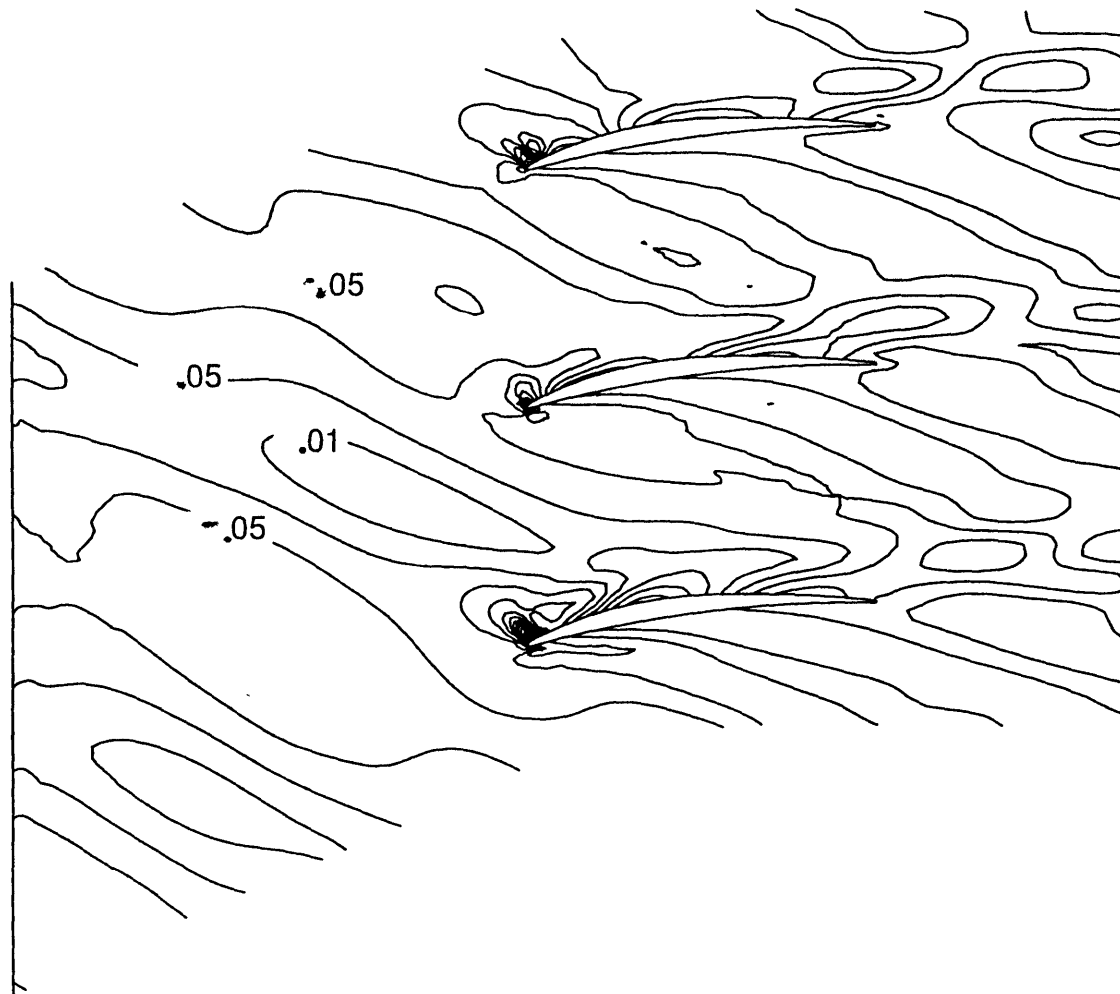
Figure 19. Test Fan Contour Plot of Perturbation Mach Number with No Suction (Wake Data at 2 Chordlengths Downstream of Rotor).

42
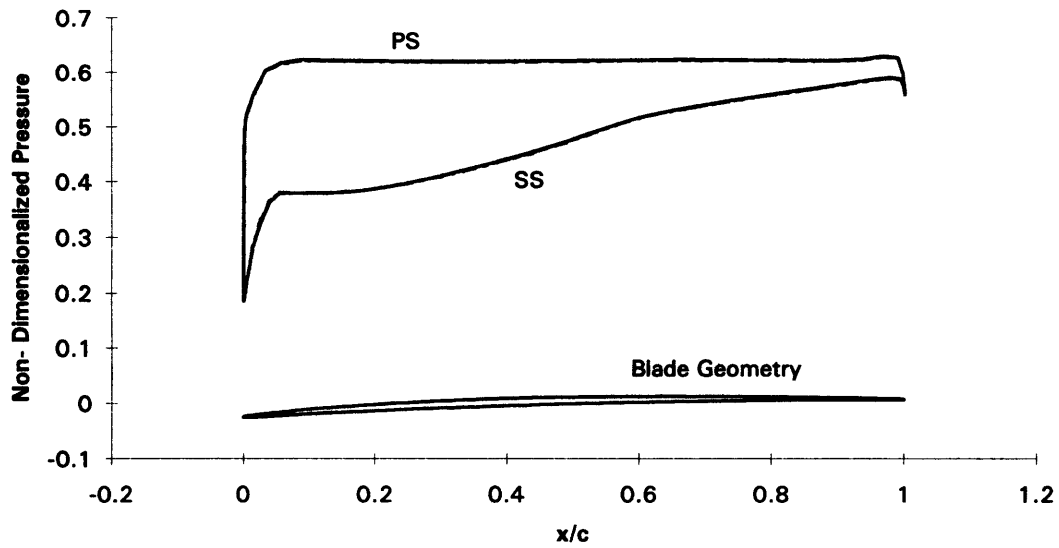
Figure 20. Test Fan Time Averaged Pressure Profile. (Note: Pressure Non-Dimensionalized wrt Stagnation Density and Speed of Sound.)
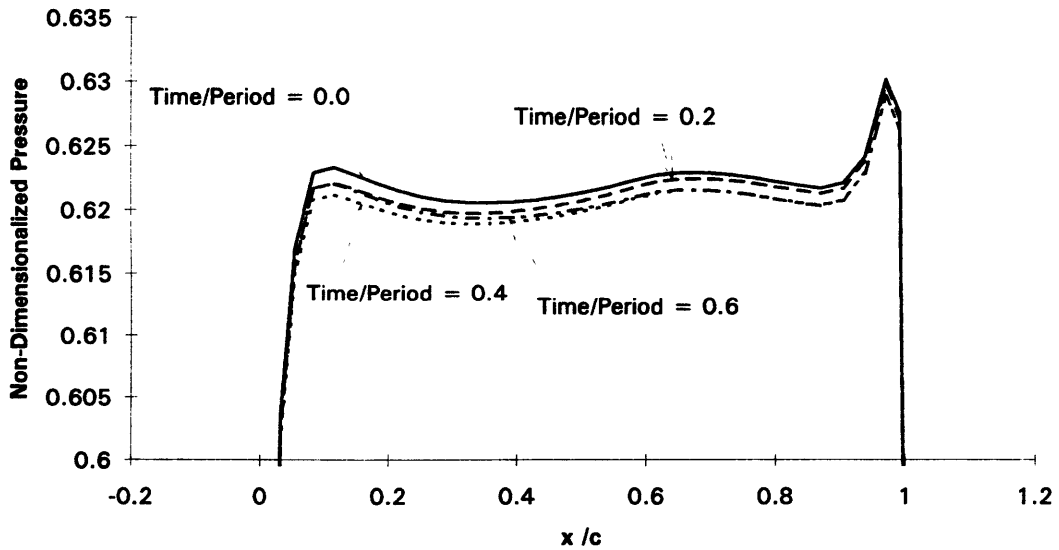
Figure 21. Magnification of Test Fan Pressure Profile Perturbations with Time. (Note: Pressure Non-Dimensionalized wrt Stagnation Density and Speed of Sound.)

43

4.2 Stage 67

In this section the impacts of suction on the Stage 67 rotor are described. Figures 22 and 23 summarize the rotor wake characteristics at two and three chordlengths downstream of the rotor with varied amounts of suction along the rotor chord. The most the wake width was reduced was approximately 30%. This corresponds to the case of 75% of the momentum thickness removed at 90% chord. The maximum reduction in wake velocity deficit was approximately 28%, and corresponds to 75% removal of the momentum thickness at 50% chord.

Figures 24 and 25 show examples of displacement thickness and momentum thickness with suction. These may be compared to the baseline cases presented previously in Figures 12 and 13. Appendix C presents displacement thickness and momentum thickness plots for each of the suction cases examined.

Figures 26-31 present the unsteady stator loading data calculated in UNSFLO using the wake data from MISES as input. Because most of the wake widths were nearly equal to the magnitude of the rotor pitch, some cases with larger wake widths showed less unsteady loading on the stator. In these cases, the wakes merged together so that the deficit was effectively reduced. (See Figures 32 and 33.) For 25% boundary layer removal for example, the reduction in deficit due to suction was outweighed by the effective increase in deficit as the wakes became un-merged, and an increase in unsteady loading with suction was displayed.

The greatest reduction in unsteady loading corresponded to the case with the largest amount of velocity deficit reduction, 75% suction at 50% chord. For this case there was a 17% reduction in unsteady loading for a rotor/stator spacing of 2

44

chordlengths, and a 10% reduction for a rotor/stator spacing of 3 chordlengths. Figure 34 presents the corresponding contour plot of the perturbation Mach number. (Note that the case of suction at 80% chord for a rotor/stator spacing of 3 chordlengths performs slightly better than the same case at 90% chord, 8% reduction versus 7% reduction. This is attributed to the slightly larger velocity deficit with suction at 90% chord due to rapid growth of the laminar boundary layer near the trailing edge.)

For Stage 67, suction at a location between 50% and 80% was the most effective in reducing unsteady loading.
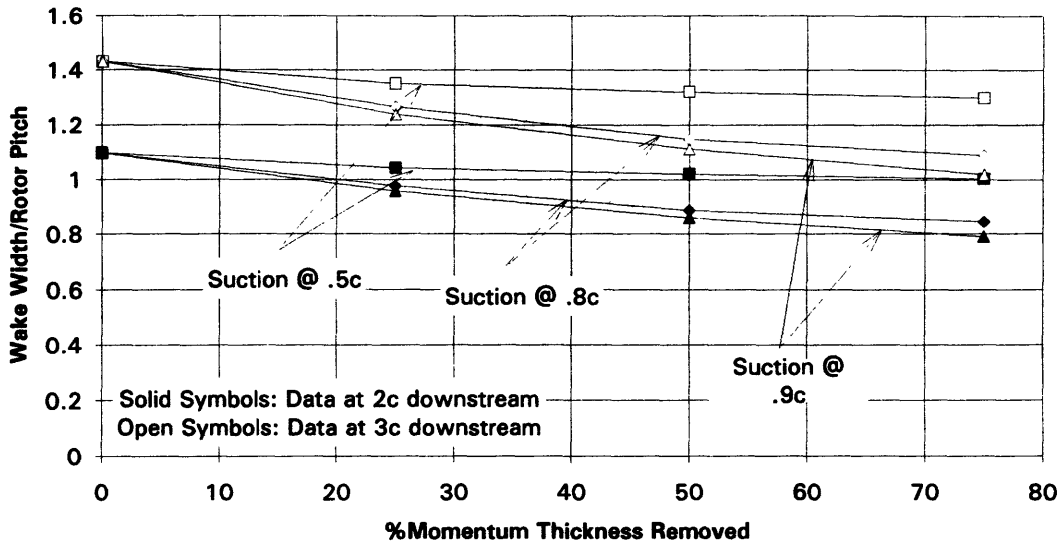
Figure 22. Stage 67 Wake Width Reduction with Suction.
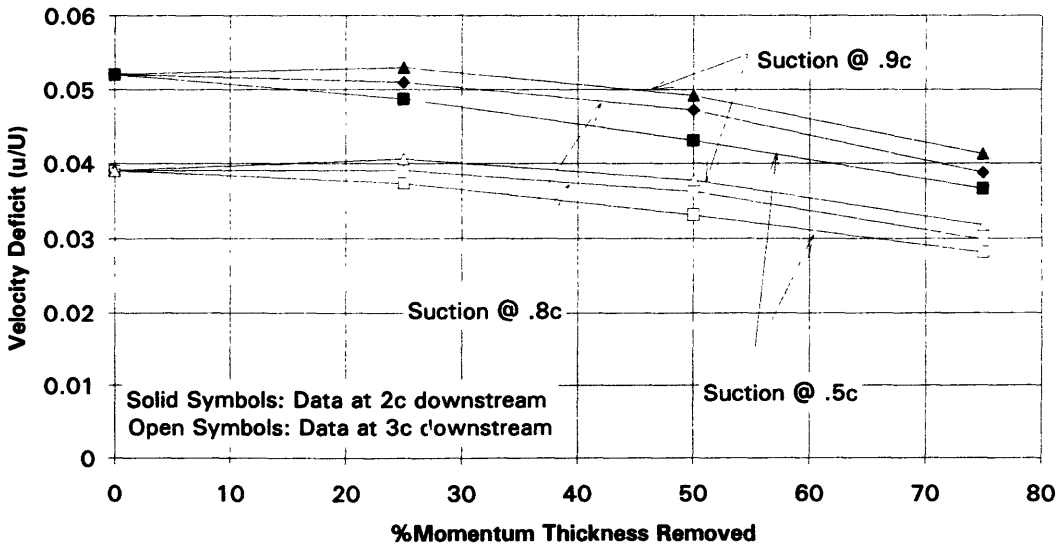
Figure 23. Stage 67 Wake Velocity Deficit Reduction with Suction.

46
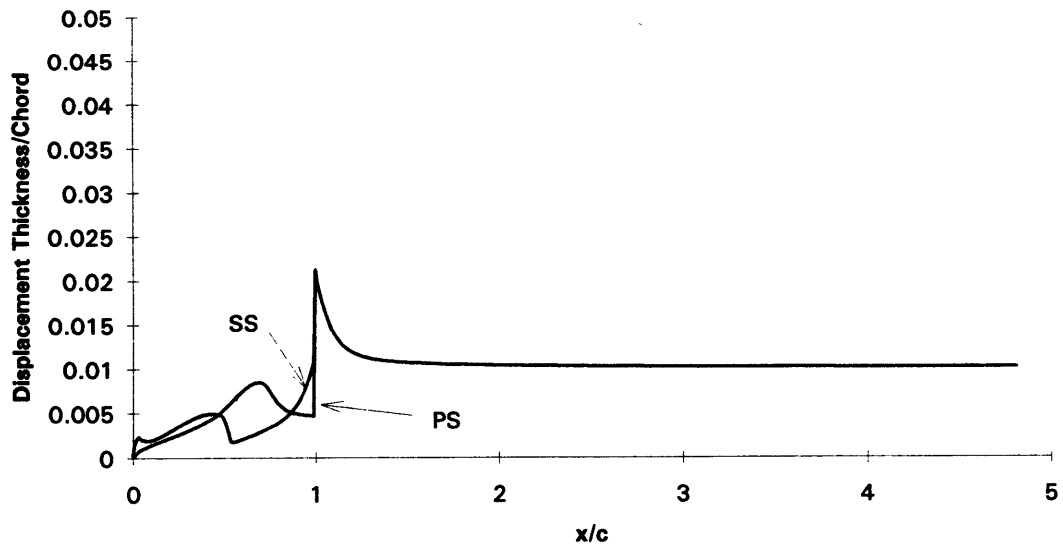
Figure 24. Stage 67 Rotor Example of Displacement Thickness with Suction.
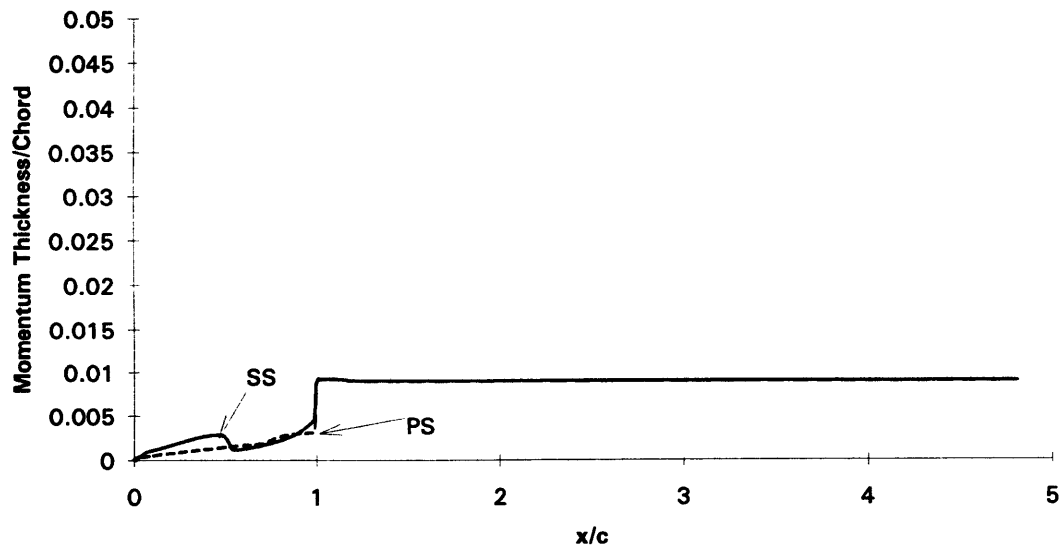
Figure 25. Stage 67 Rotor Example of Momentum Thickness with Suction.
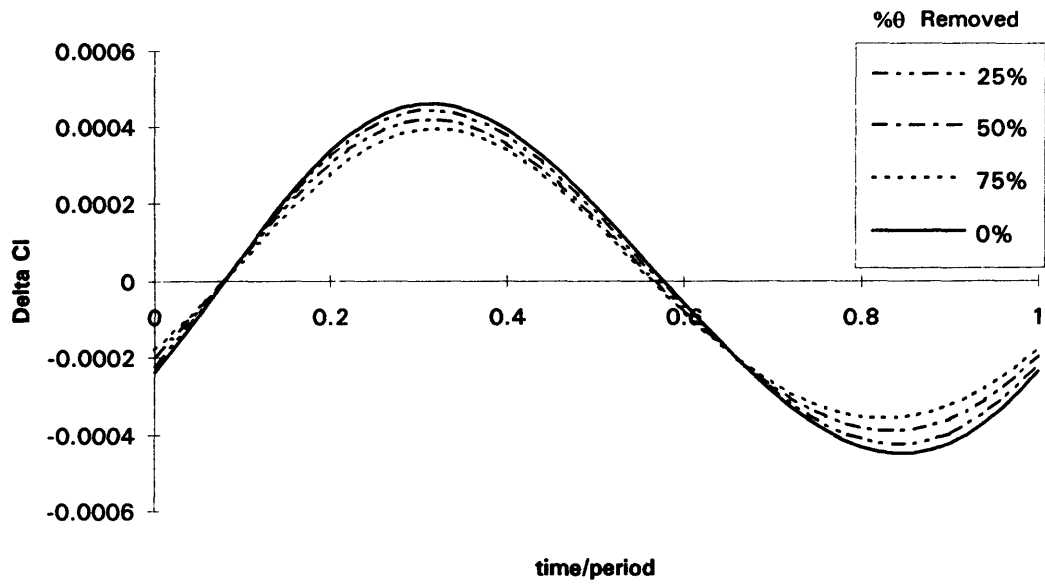
Figure 26. Stage 67 Unsteady Stator Loading for Suction at 50% Rotor Chord - Wake Data at 2 Chordlengths Downstream of Rotor.
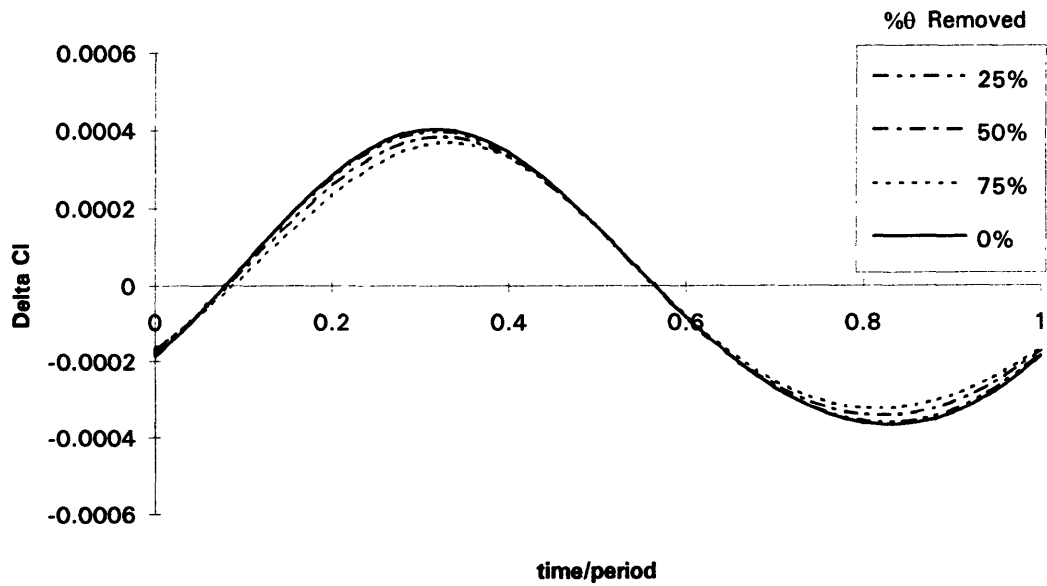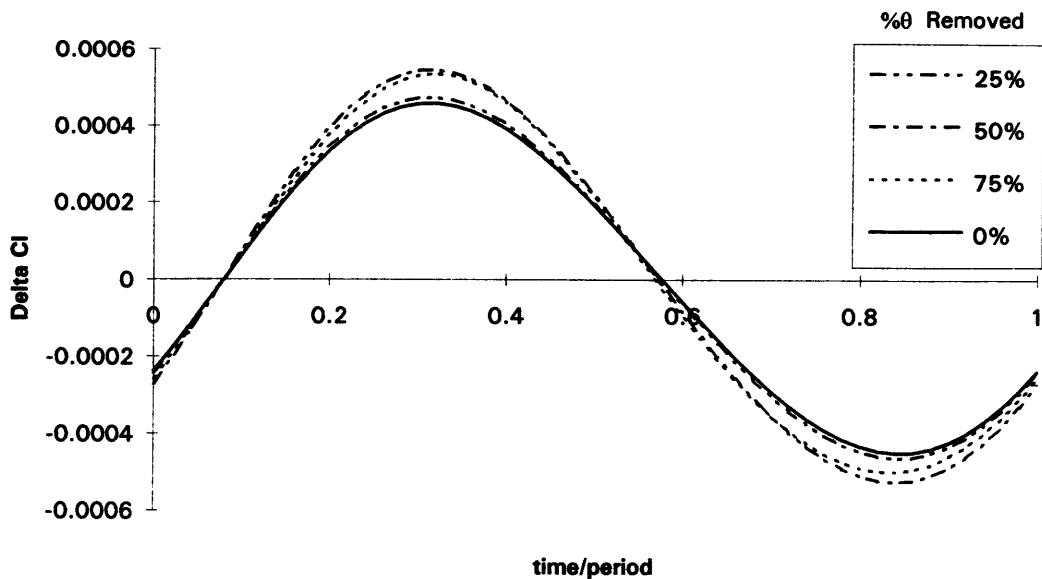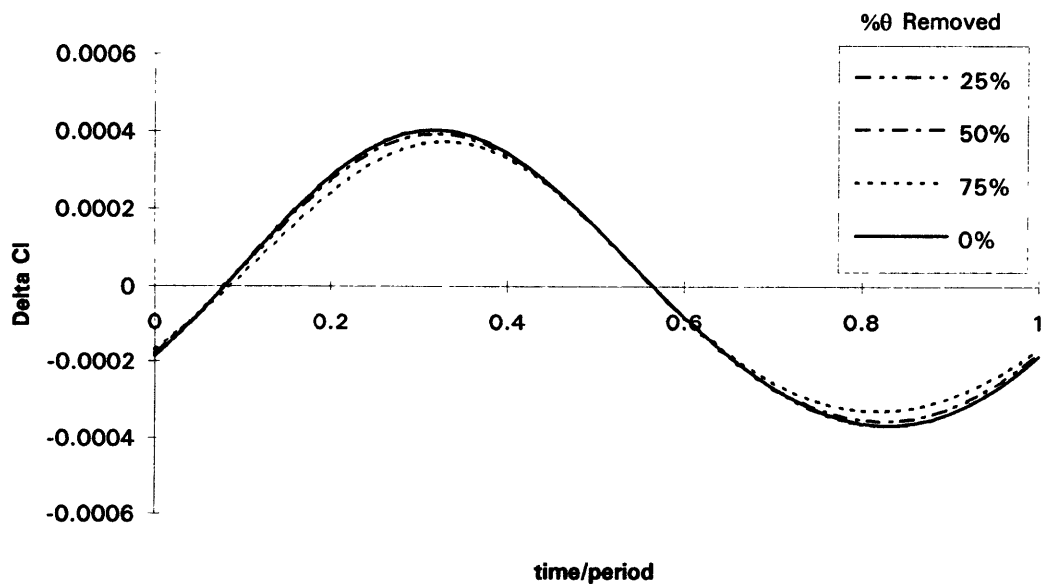

Figure 27. Stage 67 Unsteady Stator Loading for Suction at 50% Rotor Chord - Wake Data at 3 Chordlengths Downstream of Rotor.
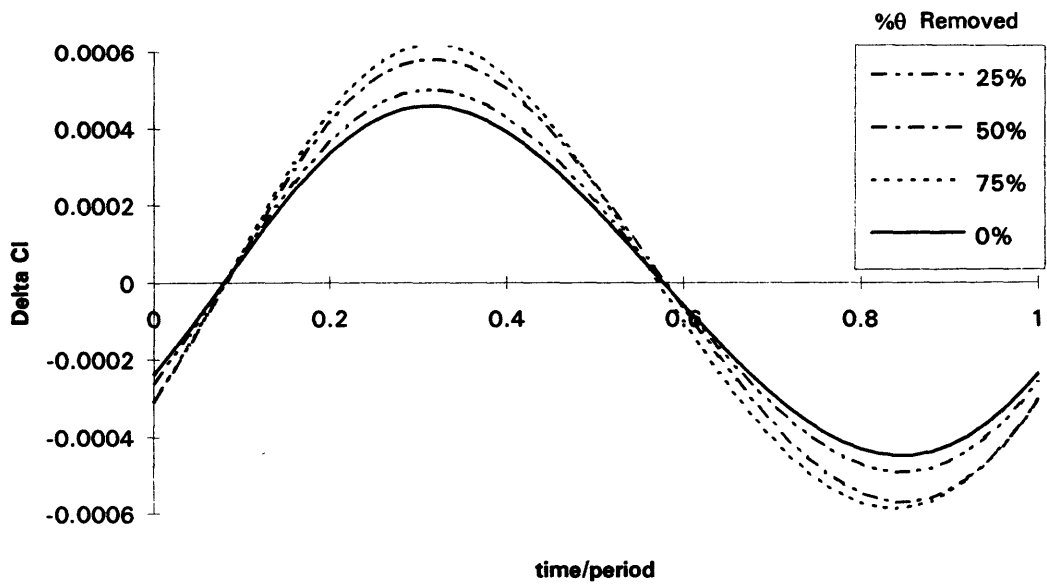
Figure 28. Stage 67 Unsteady Stator Loading for Suction at 80% Rotor Chord - Wake Data at 2 Chordlengths Downstream of Rotor.
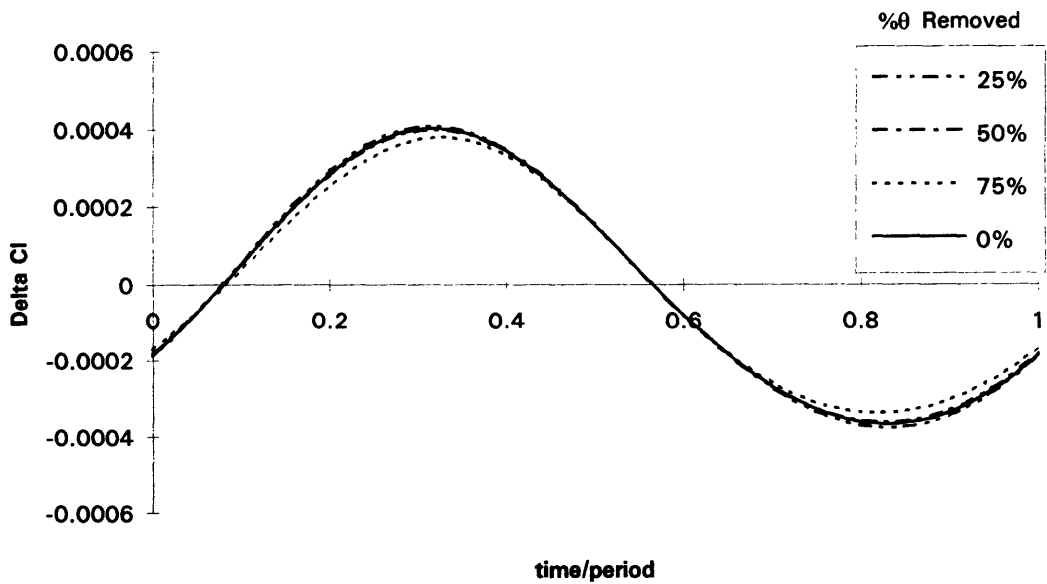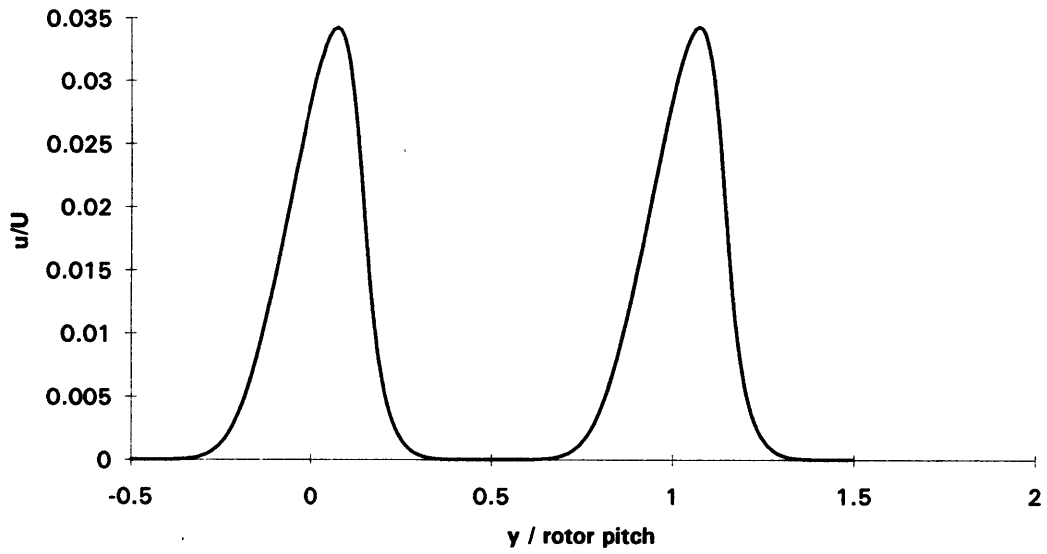

Figure 29. Stage 67 Unsteady Stator Loading for Suction at 80% Rotor Chord - Wake Data at 3 Chordlengths Downstream of Rotor.

Figure 30. Stage 67 Unsteady Stator Loading for Suction at 90% Rotor Chord - Wake Data at 2 Chordlengths Downstream of Rotor.

Figure 31. Stage 67 Unsteady Stator Loading for Suction at 90% Rotor Chord - Wake Data at 3 Chordlengths Downstream of Rotor.

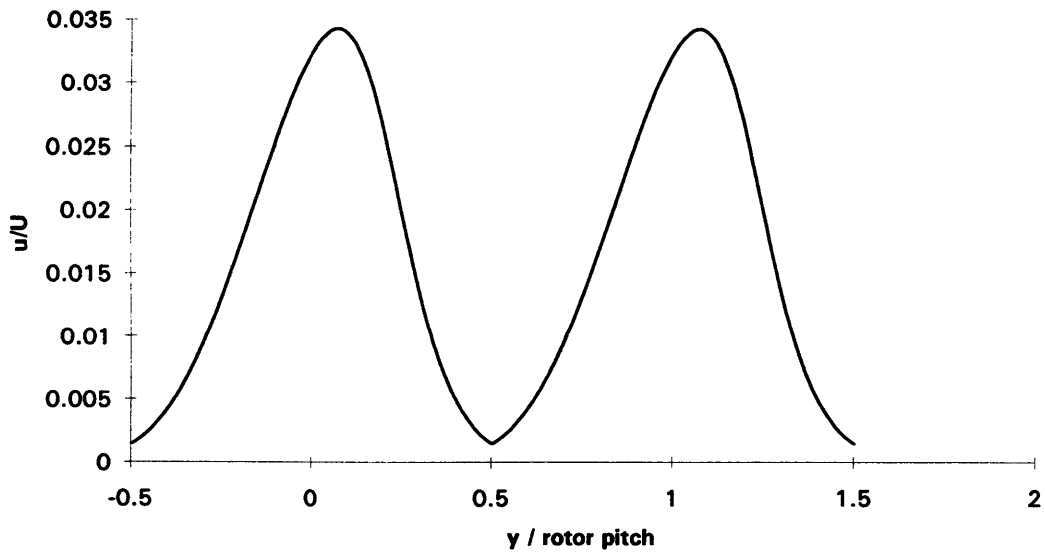**Figure 32. UNSFLO Wake Model, Velocity Deficit = 0.4, Wake Width = .5 Rotor Pitch.**

Figure 33. UNSFLO Wake Model, Velocity Deficit = 0.4, Wake Width = Rotor Pitch.
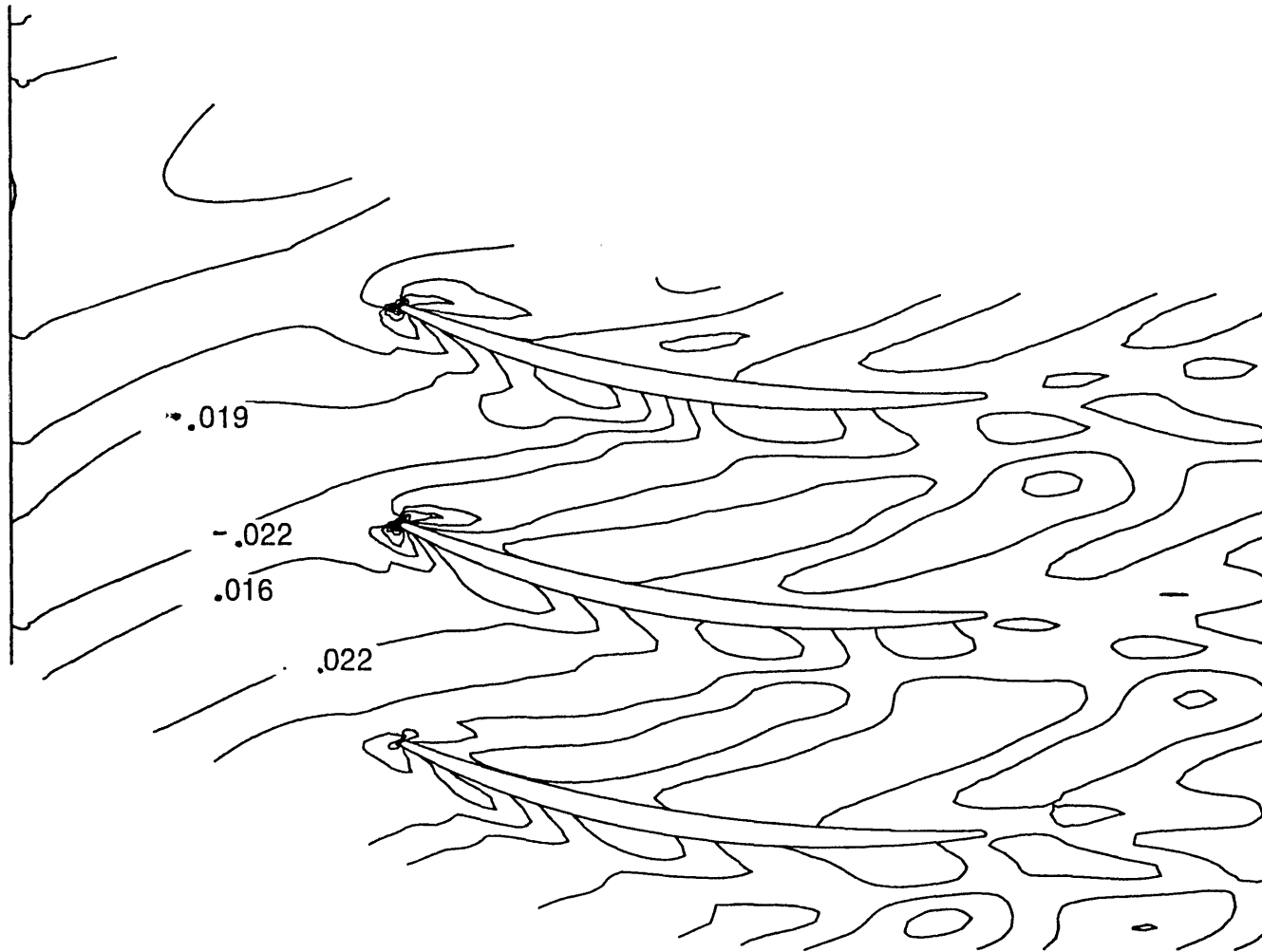
.019

-.022

.016

.022

Figure 34. Stage 67 Contour Plot of Perturbation Mach Number for 75% Suction at 50%c.

4.3 Test Fan Geometry

Figures 35 and 36 present examples of displacement thickness and momentum thickness for the Test Fan rotor with suction. These can be compared to Figures 16 and 17 presented in Section 4.1 for the baseline condition without suction. Appendix C contains a complete listing of displacement thickness and momentum thickness plots for each suction case. Figures 37 and 38 summarize the plots found in Appendix C.

Figure 37 shows that the maximum reduction of the wake width was approximately 18%. The amount the wake width can be reduced was limited by the pressure side contribution to the wake and the trailing edge thickness, which is directly added to the displacement thickness at the trailing edge. The maximum reduction of the velocity deficit achievable was approximately 40%. This, similarly, is limited by the pressure side and trailing edge contributions to the wake. Although the impact of suction in this model-scale rotor was limited by the trailing edge thickness, suction in a full-scale fan rotor may not encounter such limitations because the trailing edge thickness will not scale directly.

The results from the wake study summarized in Figures 37 and 38 were used as input to UNSFLO to calculate unsteady loading on the stator. Figures 39-44 present a summary of the stator unsteady loading calculations done using UNSFLO. The unsteady response for this stage was nearly sinusoidal. This was due to the combination large rotor/stator pitch ratio and wake widths nearly as large as the rotor passages, such that there was approximately one wake in a stator passage at any time. The results suggests that the maximum achievable reduction of the unsteady loading on the stator is approximately 25%. This corresponds to the case with 75% suction at 80% chord with

wake data for a rotor/stator spacing of 2 rotor chordlengths. Figure 45 presents a contour plot of the perturbation Mach number for this case.

Similar to the Stage 67 results, the data also shows some interesting characteristics when the wake width is nearly as large as the rotor pitch. Cases with larger wake widths sometimes showed less unsteady loading on the stator. This occurred because the natural wake width was larger than the rotor spacing and the wakes merged together so that the deficit was effectively reduced. (See Figures 32 and 33.) With small amounts of suction, the increase in effective deficit due to un-merging was larger than the decrease due to suction.

Figure 46 shows unsteady loading data obtained from the Kemp and Sears model (See summary in Appendix A) using wake data for suction at 90% chord. The results show a reduction in unsteady loading of approximately 35%. This was 10% more reduction than the UNSFLO calculations predicted, but recall that the UNSFLO calculations take into account many effects which are not included in the Kemp and Sears analysis (which models incompressible flow over a thin, isolated airfoil).
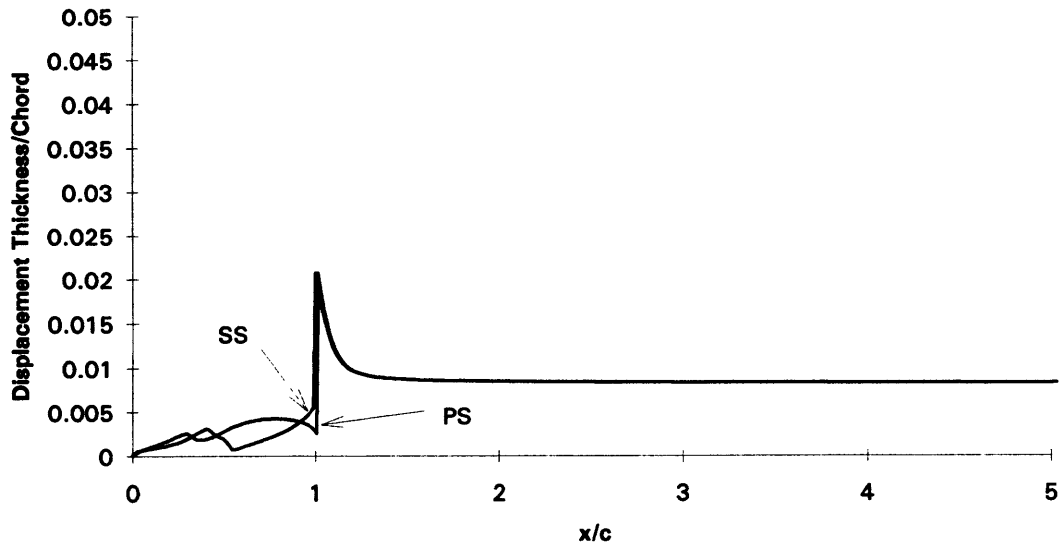
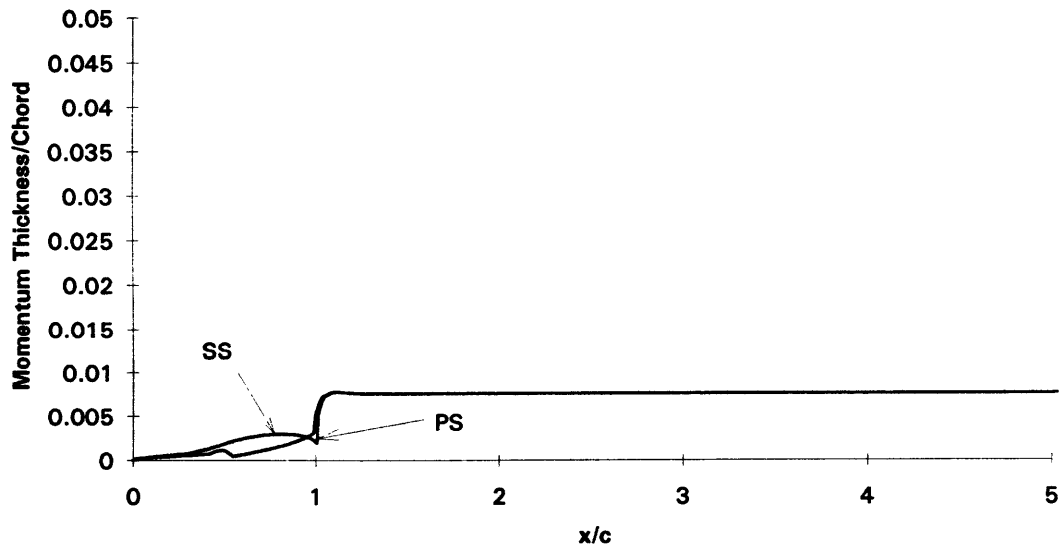**Figure 35. Test Fan Rotor, Example of Displacement Thickness With Suction.**

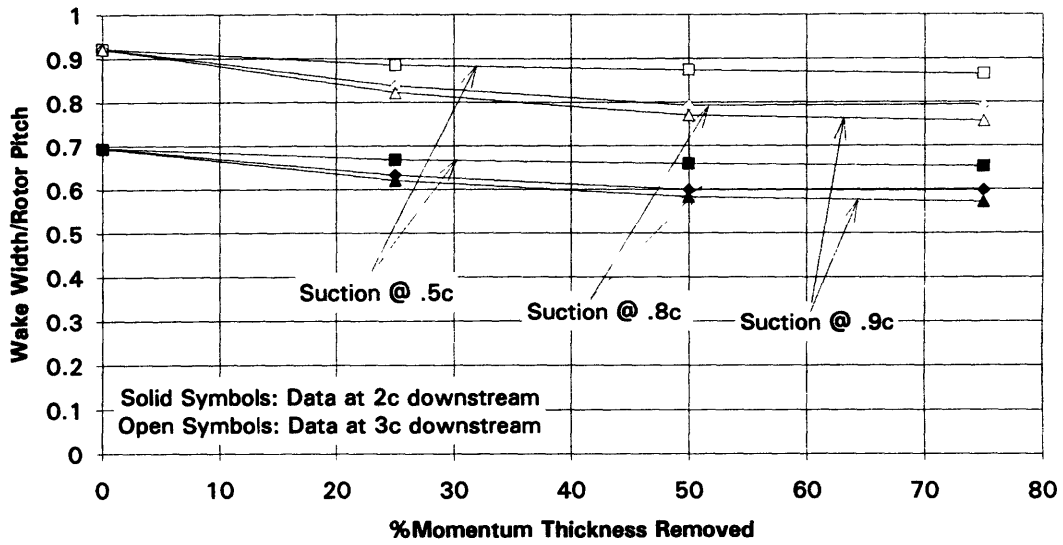**Figure 36. Test Fan Rotor, Example of Momentum Thickness With Suction.**

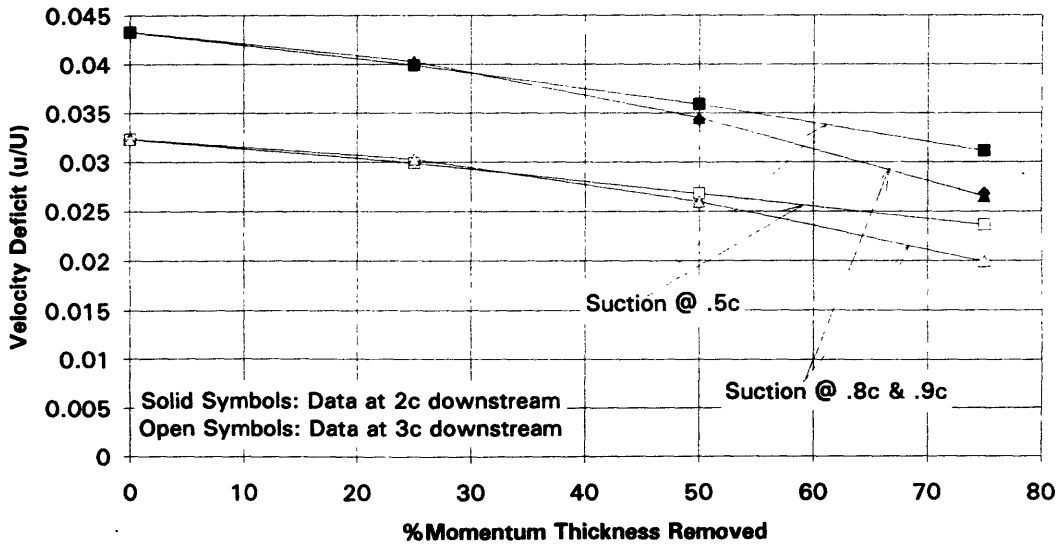**Figure 37. Test Fan Wake Width Reduction from Suction.**

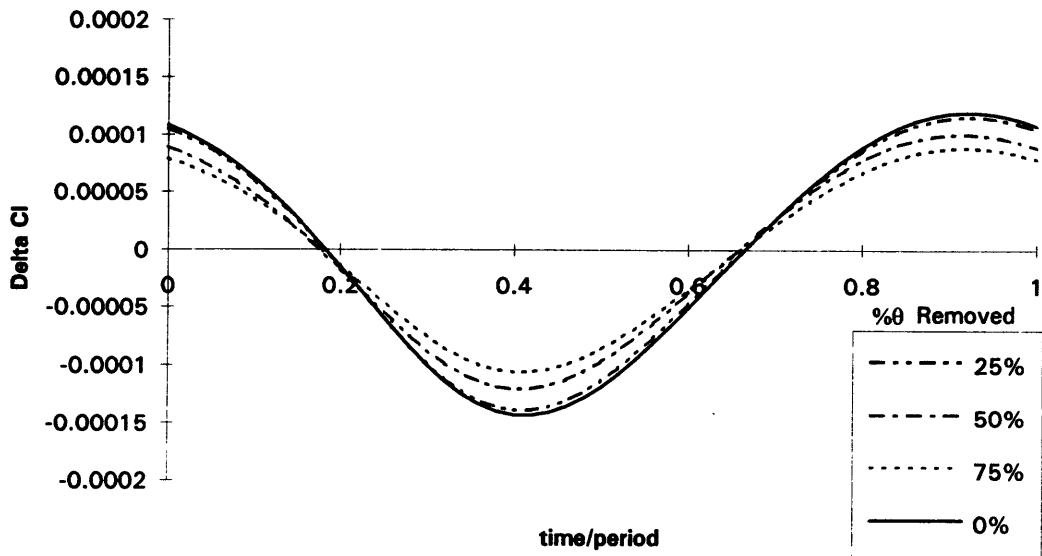**Figure 38. Test Fan Wake Velocity Deficit Reduction with Suction.**

**Figure 39. Test Fan Unsteady Stator Loading for Suction at 50% Rotor Chord -
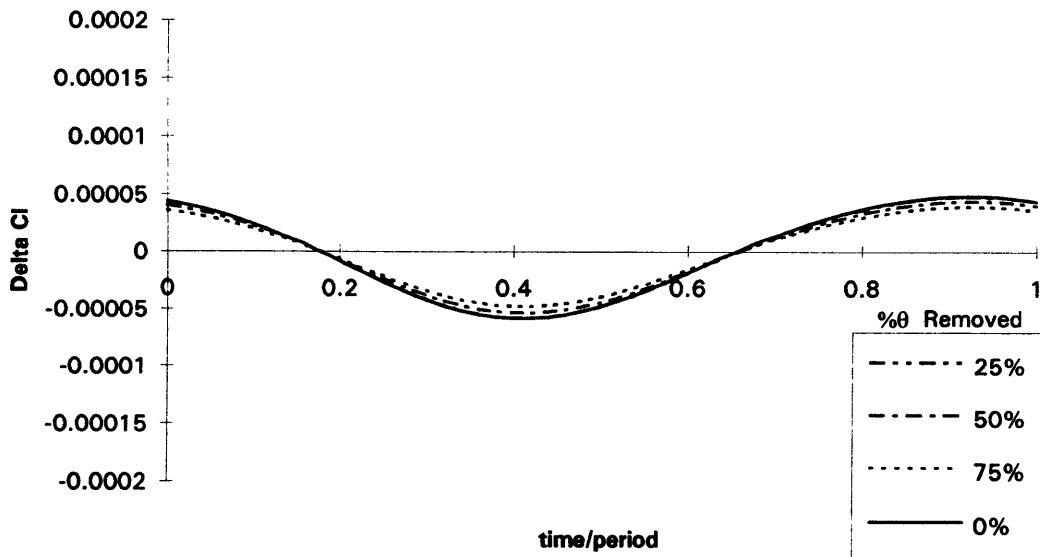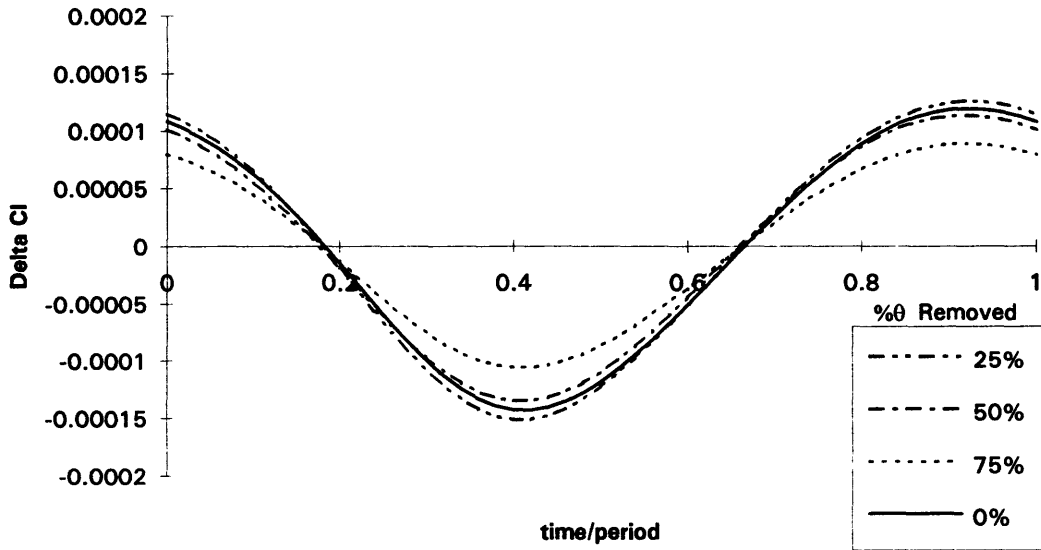Wake Data at 2 Chordlengths Downstream of Rotor.**

**Figure 40. Test Fan Unsteady Stator Loading for Suction at 50% Rotor Chord -
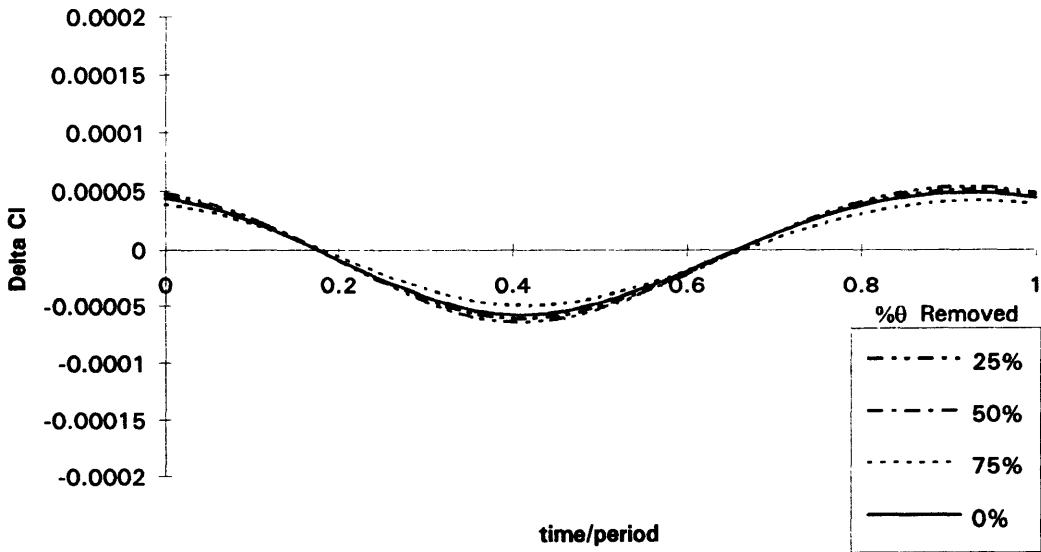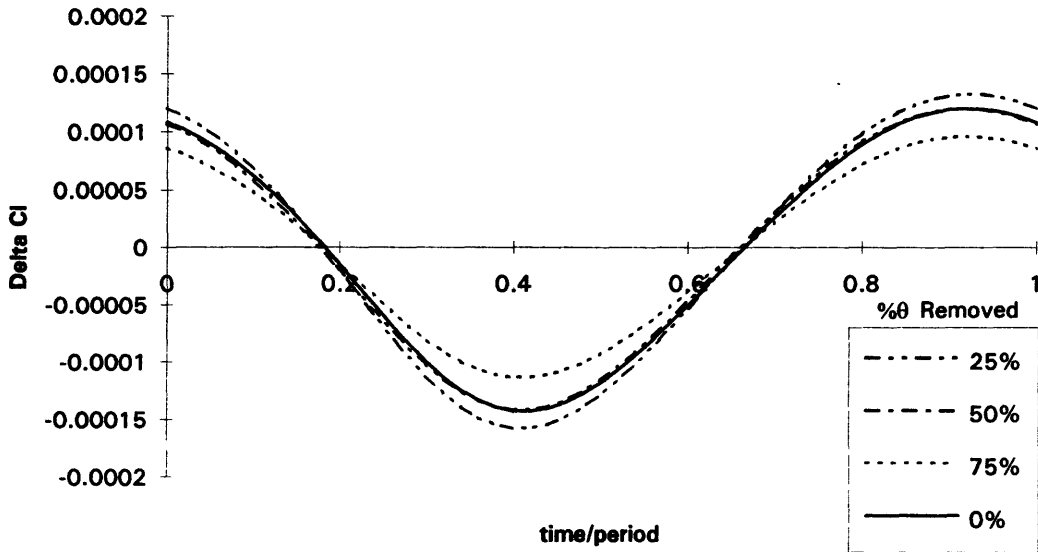Wake Data at 3 Chordlengths Downstream of Rotor.**

57

Figure 41. Test Fan Unsteady Stator Loading for Suction at 80% Rotor Chord - Wake Data at 2 Chordlengths Downstream of Rotor.

Figure 42. Test Fan Unsteady Stator Loading for Suction at 80% Rotor Chord - Wake Data at 3 Chordlengths Downstream of Rotor.
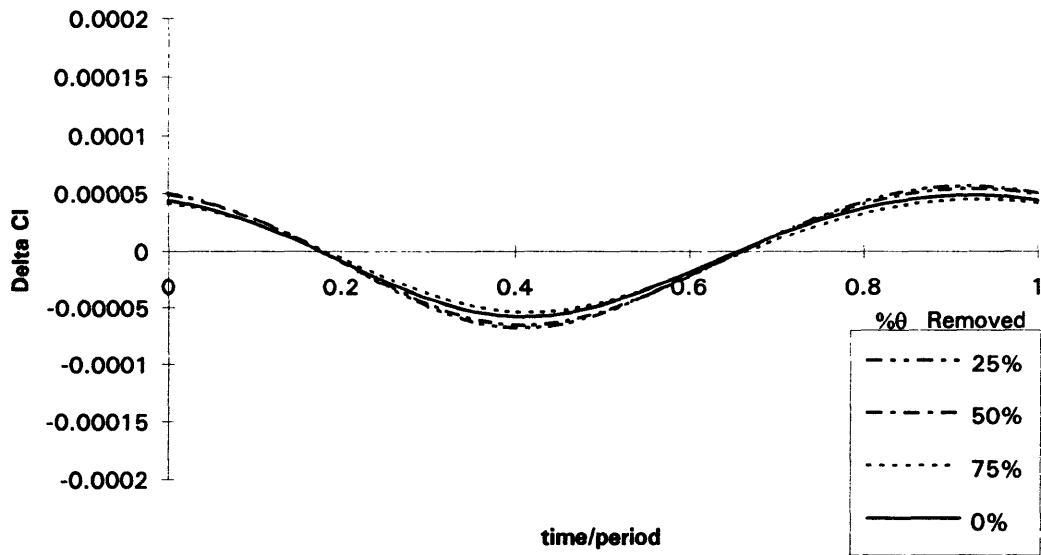
58

Figure 43. Test Fan Unsteady Stator Loading for Suction at 90% Rotor Chord - Wake Data at 2 Chordlengths Downstream of Rotor.

Figure 44. Test Fan Unsteady Stator Loading for Suction at 90% Rotor Chord - Wake Data at 3 Chordlengths Downstream of Rotor.
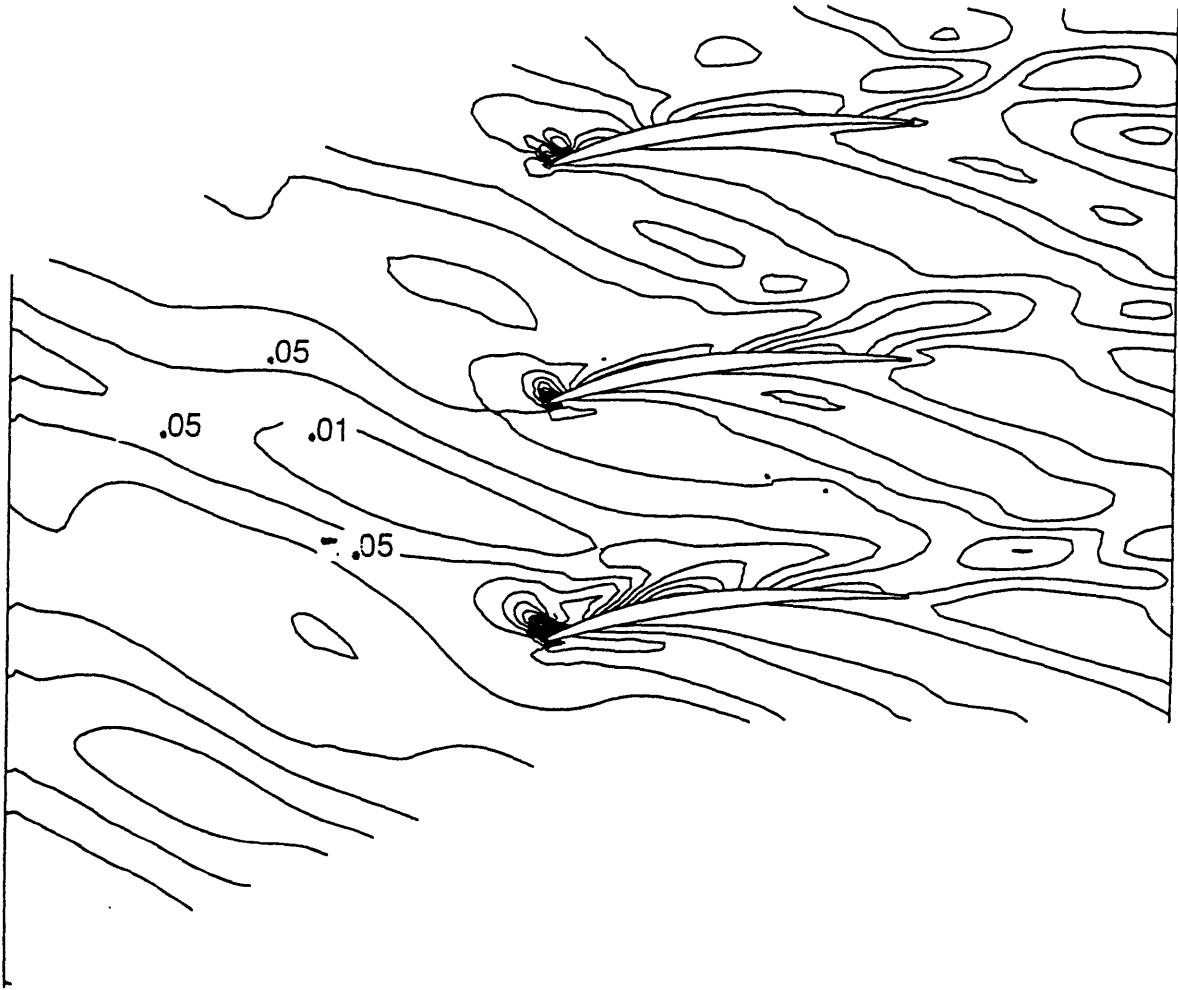
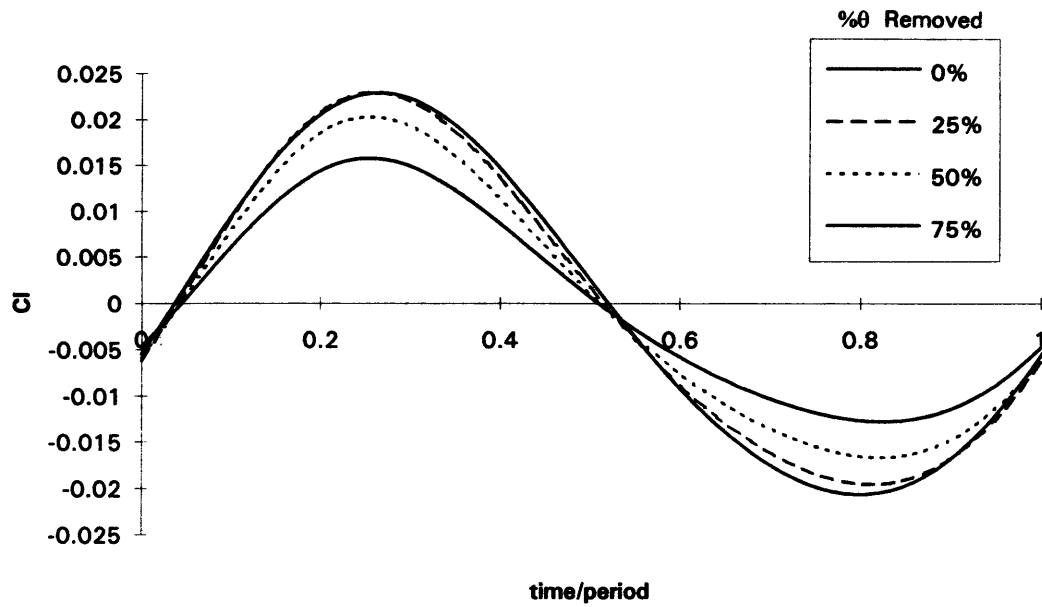**Figure 45. Test Fan Contour Plot of Perturbation Mach Number for 75% Suction at 80%c.**

Figure 46. Example of Kemp and Sears Unsteady Loading Model Using Wake Data for Suction at 90% Chord.

4.4 Transducer placement study.

An analysis of the unsteady loading results from UNSFLO was performed to give

insight into the number and appropriate location of transducers necessary to resolve the

unsteady loading on the stator for future experiments in the MIT Blowdown Compressor.

The pressure at each of approximately 95 grid points along the Test Fan stator

blade was obtained from the UNSFLO calculations for the case with no suction and a

rotor/stator axial spacing of two rotor chordlengths. The unsteady loading obtained by

integrating the pressure at all of the grid points was compared to that obtained using only

selected points. The selected points were used to model the experimental data which

would be available using a limited number of transducers. Figure 47 shows a case where

six transducers were located on each surface of the blade. Various other combinations of

location and number of transducers were examined as well. Figure 48 shows pressure

data versus chord for the case of 95 grid points and six transducers per side. The

pressures at the leading and trailing edges were assumed to be equal to that at the nearest

transducer. Using this assumption, inlet and exit pressure data are not needed, and all

calculations can be made with transducer data only.

Figure 49 shows that using 6 transducers, one at 8% chord, one at 90% chord, and

four equally spaced between them, yielded errors of approximately 8% in magnitude of

unsteady loading from the case when all 95 data points are used. Most of this error was

incurred by the physical limitations of locating transducers near the leading edge of the

blade. This is demonstrated in Figure 49 which shows that if all the data points at the

leading edge between the 8% chord pressure side transducer and the 8% chord suction

side transducer were used, the error drops to approximately 2% with a slight overshoot.

The overshoot is due to the assumption that the pressure at the trailing edge is the same as

the pressure at the transducer nearest the trailing edge of the blade.

In conclusion, this study showed that using six transducers on both sides of the

blade yields an error in measuring unsteady loading of approximately 8%, and that

placing more transducers near the leading edge improves the measurement accuracy.

Computational Grid Point

Transducer Location
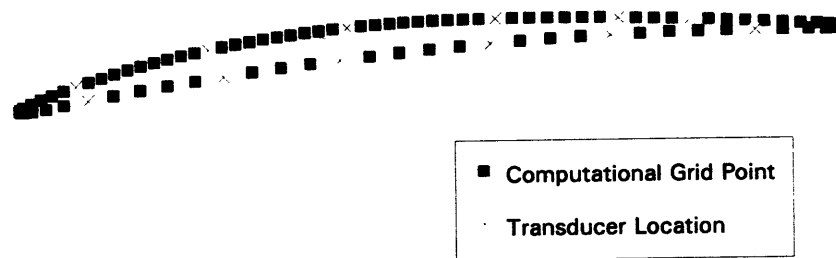
Figure 47. Test Fan Transducer Locations for Transducer Placement Study.
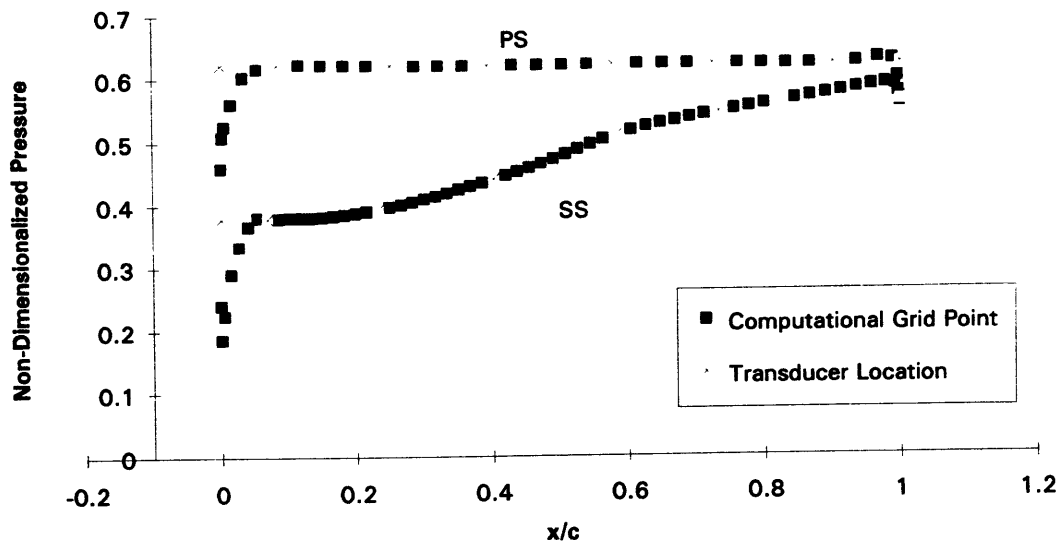
Figure 48. Sample of Pressure Data at a Given Instant of Time Used to Calculate Unsteady Loading on the Stator. (Note: Pressure Non-Dimensionalized wrt Stagnation Density and Speed of Sound.)
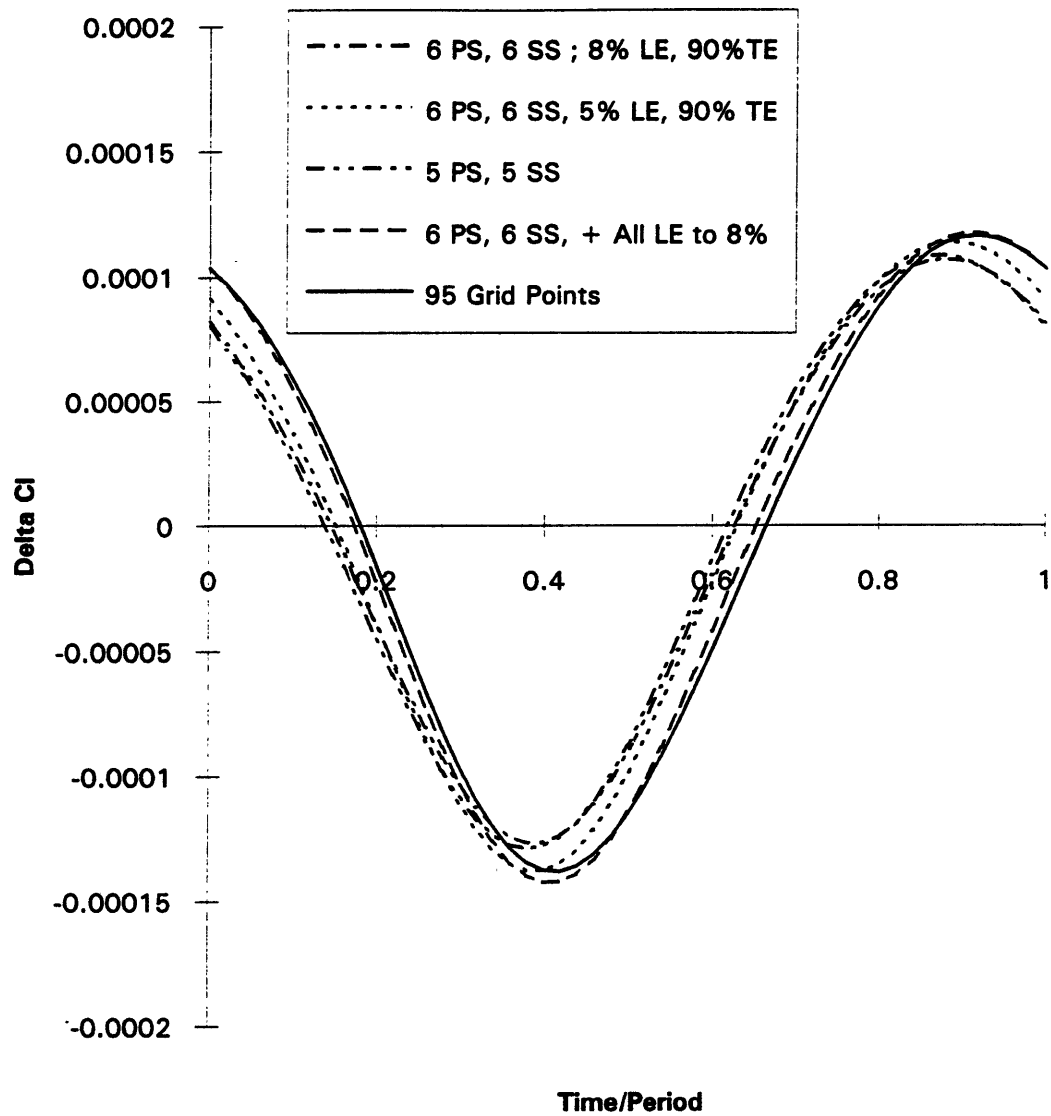
Figure 49. Unsteady Loading on Stator with Various Transducer Configurations.

Chapter 5

5.0 Summary and Conclusions

A new method for reducing fan rotor/stator interaction noise was examined. The method employs rotor blade boundary layer suction to reduce the magnitude and scale of the wakes shed by the rotor, thereby reducing the unsteady loading on the stator. A two-dimensional, computational analysis was performed to determine the dependence of unsteady stator loading on the amount of fluid removed, the location along the rotor chord at which the fluid was removed, and the rotor/stator axial spacing. A study of the unsteady loading on the stator was also completed to determine the optimum number and location of transducers needed to accurately resolve unsteady loading on the stator for future experiments in the MIT Blowdown Compressor.

The thickness of the rotor blade trailing edge had a significant impact on the effectiveness of suction in reducing the size of the rotor wakes. For the geometry with the smaller trailing edge thickness (Stage 67 Rotor), the wake width at 2 chordlengths downstream of the rotor was reduced by approximately 30%, and the velocity deficit was reduced by approximately 28%. For the Test Fan geometry, where the trailing edge

thickness was approximately equal to the suction side boundary layer displacement thickness, the wake width was reduced by 21%, and the velocity deficit was reduced by approximately 40% (at a position of 2 chordlenghts downstream of the rotor trailing edge).

The impact of rotor boundary layer suction on stator unsteady loading was also dependent on the geometry of the stage. When the wakes were larger than the rotor pitch, they merged, effectively reducing the velocity deficit. For cases with small amounts of suction (*e.g.* 25%), the increase in effective deficit due to un-merging of the wakes outweighed the decrease in deficit due to boundary layer removal so that the unsteady loading was increased.

For larger suction levels unsteady loading reductions were demonstrated. The largest loading reduction achieved for the Stage 67 geometry was approximately 10%. This occurred for suction locations between 50% and 80% chord. The largest reduction in loading for the Test Fan was approximately 25%. This corresponded to 75% suction at 80% and 90% chord. Though the trailing edge thickness of the Test Fan was nearly equal to the suction surface boundary layer displacement thickness, the unsteady loading for the Test Fan geometry was reduced more than that for the Stage 67 geometry because more velocity deficit reduction was achieved with boundary layer suction for the Test Fan geometry.

This study was performed at a midspan section for each geometry. Studies along the entire blade should be completed to obtain a more comprehensive understanding of this wake management strategy. Acoustic calculations and measurements are also necessary to determine the impact of this wake management technique on radiated noise.

Further, cycle studies need to be performed to determine any performance

penalties/benefits associated with suction and blowing.

List of References

[1]   Kantola, R.A., and Gliebe, P.R., "Effects of Vane/Blade Ratio and Spacing on Fan
        Noise," AIAA-81-2033, October, 1981.

[2]   Kemp, N.H., "On the Lift and Circulation of Airfoils in Some Unsteady-Flow
        Problems," Journal of the Aeronautical Sciences, Vol. 19, No. 10, p. 713, October,
        1952.

[3]   Kemp, N.H., and Sears, W.R., "The Unsteady Forces Due to Viscous Wakes in
        Turbomachines," Journal of the Aeronautical Sciences, July, 1955.

[4]   Sears, W.R., "Some Aspects of Non-Stationary Airfoil Theory and Its Practical
        Application," Journal of the Aeronautical Sciences, Vol. 8, No. 3, pp. 104-108,
        January, 1941.

[5]   Silverstein, A., Katzoff, S., and Bullivant, W.K., "Downwash and Wake Behind
        Plain and Flapped Airfoils," NACA Rep. 651, 1939.

[6]   Amiet, Roy K., "Compressibility Effects in Unsteady Thin-Airfoil Theory," AIAA
        J., vol. 12, no. 2, Feb. 1974, pp.252-255.

[7]   Goldstein, M.E. and Atassi, H., "A Complete Second-Order Theory for the
        Unsteady Flow About an Airfoil Due to a Periodic Gust," J. Fluid Mech., vol. 74,
        pt. 4, Apr. 22, 1976, pp.741-765.

[8]   Namba, M., "Three-Dimensional Analysis of Blade Force and Sound Generation
        for an Annular Cascade in Distorted Flows," J. Sound & Vibration, vol. 50, no. 4,
        Feb. 22,1977, pp.479-508.

[9]   Epstein, A.H., Giles, M.B., Shang, T., and Sehra, A.K., "Blade Row Interaction
        Effects on Compressor Measurements," AGARD CP 468,

[10]   Groeneweg, J.F., Sofrin, T.G., Rice, E.J., and Gliebe, P.R., "Aeroacoustics of
        Flight Vehicles: Theory and Practice; Volume 1: Noise Sources; Turbomachinery
        Noise," NASA RP 1258, August, 1991.

[11]   Waitz, I.A., Personal communication, Sept. 1992.

[12]   Drela, M., "Two-Dimensional Transonic Aerodynamic Design and Analysis
        Using the Euler Equations," GTL Report #187, February, 1986.

[13] Giles, M., "UNSFLO: A Numerical Method for the Calculation of Unsteady Flow in Turbomachinery," GTL Report 205, May 1991.

[14] Strazisar, A.J., "Laser Anemometer Measurements in a Transonic Axial Flow Fan Rotor," NASA TP-2879, November 1989.

[15] Hathaway,, M.D., "Rotor Wake Characteristics of a Transonic Axial Flow Fan," AIAA Paper No. 85-1133, 1985.

[16] Topol, D.A., and Philbrick, D.A., "Fan Noise Prediction System Development: Wake Model Improvements and Code Evaluations," NASA Informal Report, April, 1993.

[17] Youngren, H., and Drela, M., "A User's Guide to MISES V1.2," (unpublished), September, 1992.

[18] Giles, M., Haimes, R., "UNSFLO User's Manual Version 5.3," (unpublished), August 1990

[19] Manwaring, S.B., and Wisler, D.C., "Unsteady Aerodynamics and Gust Response in Compressors and Turbines," ASME, International Gas Turbine and Aeroengine Congress and Exposition, 37th, Cologne, Germany, June 1-4, 1992.

[20] Urasek, D.C., Gorrell, W.T., Cunnan, W.S., "Performance of Two-Stage Fan Having Low-Aspect Ratio, First-Stage Rotor Blading," NASA TP 1493, Aug 1979.

[21] von Karman, T.H., and Sears, W.R., "Airfoil Theory for Non-Uniform Motion," Journal of the Aeronautical Sciences, Vol. 5, No. 10, pp.379-390, August, 1938.

Appendix A

Gust response of an airfoil.

An analytical model of unsteady forces on airfoils developed by Kemp and Sears was used. It is derived from incompressible, two-dimensional thin airfoil theory, and was used to determine unsteady loading on a blade row due to an upstream wake.

Using theories developed for gust-response on airfoils [Ref. 4], an expression for unsteady lift on an airfoil due to a velocity perturbation is defined. This assumes that the upwash velocity into the airfoil is periodic and has the form of:

$$v(x,t) = v_o e^{i\omega(t-x/U)}$$

The unsteady lift and moment response to a gust of this form is found to be

$$L(t) = 2\rho V v_o S(\omega) e^{i\eta t}$$

$$M(t) = \frac{L(t)}{2c}$$

where $S(\omega)$ is the Sears' function and is defined as

$$S(\omega) = \frac{1}{i\omega\left[K_0(i\omega) + K_1(i\omega)\right]}$$

This model takes into account the quasi-steady lift, the lift due to the vorticity distribution in the wake and the lift if there were no wake and the only forces acting on the body were those due to it moving through an ideal fluid.

Unsteady loading on a cascade due to viscous wakes.

Ref. 11 takes this a step further and applies the gust response model to a stator/rotor with viscous wakes. Expressions for wake profiles developed by Silverstein

71

[Ref. 5] and are used to define the velocity profile in the wake. The equations used to

describe the wakes are

Half-width of wake: $\quad Y = 0.68\sqrt{2}c_s\left(C_d\dfrac{x'}{c}\right)^{1/2}$

Velocity deficit: $\quad \dfrac{u_c}{U} = \dfrac{-2.42\sqrt{C_d}}{\dfrac{x'}{c}+0.3}$

Velocity Profile: $\quad \dfrac{u}{u_c} = \cos^2\left[\dfrac{\pi}{2}\dfrac{y}{Y}\right]$

The wake velocity profile is assumed to be symmetric and is approximated with a

Gaussian profile and is only valid inside the wake (y<Y):

$$\frac{u}{u_c} = e^{-\pi\left(\frac{y'\cos\alpha}{Y}\right)^2}$$

For a cascade of wakes and stators, the total velocity field becomes

$$\frac{u_T}{u_c} = \sum_{n=-\infty}^{\infty} e^{-\pi\left(\frac{\cos\alpha}{Y}\right)^2(y'-nd)^2}$$

where d is the pitch of the wakes.

The Fourier series of this yields the following equation for wake profile:

$$\frac{u_T}{u_c} = \frac{2\sqrt{\pi}}{K}\sum_{m=1}^{\infty} e^{-2\pi i m\frac{y}{d}-\frac{\pi^2 m^2}{K^2}}$$

where

$$K \equiv \pi\cos^2\alpha\left(\frac{d}{Y}\right)^2$$

The y-component of this is $u_T\sin\beta$, and the upwash velocity on the stator due to the wakes

is of the form:

$$v(x,t) = \frac{1}{2\pi} U \sum_{m=1}^{\infty} G_m e^{ivm(t-x/U)}$$

where

$$G_m \equiv 4\pi \frac{V_r}{V_s} \frac{2.42\sqrt{C_d}\sin\beta}{x'/c + 0.3} \frac{0.68\sigma}{\sqrt{2}\cos\alpha} \sqrt{\frac{Cdx_o'}{c}} e^{-\pi m^2 \left(\frac{0.68\sigma}{\sqrt{2}\cos\alpha}\right)^2 \frac{C_d x_o'}{c}}$$

This is of a form similar to the upwash velocity defined for a gust, therefore the same

method is applied to solve for the unsteady lift. The unsteady lift coefficient ,Cl, is then

$$Cl(t) = \sum_{m=1}^{\infty} G_m S(m\omega_r) e^{imv_r t}$$

where

$$S(m\omega_r) = \frac{1}{im\omega_r [K_0(im\omega_r) + K_1(im\omega_r)]}$$

73

Appendix B

An empirical wake correlation was developed by Topol [Ref. 16] from laser anemometer data described in Ref. 15. These correlations were compared to the wake calculations made by the MISES model.

The basic equations that define this correlation are of the form

$$y = \frac{ax + b}{cx + d}.$$

The velocity deficit is defined as one-half the total velocity deficit and the wake width is the total width of the wake at the point where the velocity deficit is one-half the maximum velocity deficit. The equations derived from experimental data are:

Wake Width:
$$\frac{\delta}{S} = \frac{1.63632\left(\frac{s}{c}\right)C_d^{1/8} - 0.01944}{5.5755\left(\frac{s}{c}\right)C_d^{1/8} + 1.0}$$

and

Velocity Deficit:
$$\left(\frac{W_{dc}}{W_o}\right)\left(\frac{1}{C_d^{1/4}}\right) = \frac{1.17543\left(\frac{s}{c}\right) + 1.28626}{10.79857\left(\frac{s}{c}\right) + 1.0}$$

where W_{dc} is the wake centerline defect of total relative velocity, and W_o is the total relative velocity in the free stream. The velocity profile inside the wake is assumed to be a Gaussian profile and normalized with respect to the centerline defect of total freestream velocity:

$$\frac{W_d}{W_{dc}} = e^{-693\eta^2}$$

74

where η, the normalized tangential distance from the centerline of the rotor wake, is

defined as: $\eta = \dfrac{y}{\delta/2}$.

Appendix C

This section contains plots of displacement thickness and momentum thickness for all of the suction cases examines with each geometry. The parameters are plotted versus axial position normalized by rotor chord. The data along the chord (up to $x/c=1.0$) is the value of the parameter on the side noted (SS: suction surface, PS: pressure surface). The data in the wake ($x/c>1.0$) is the total wake width, i.e. sum of pressure surface and suction surface.
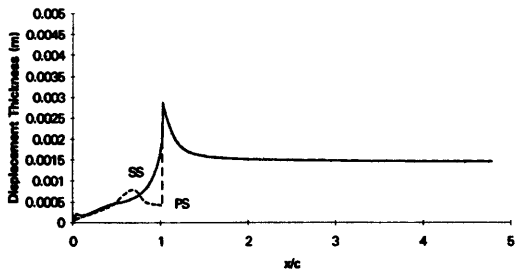
Figure C-1. Stage 67, No Suction.
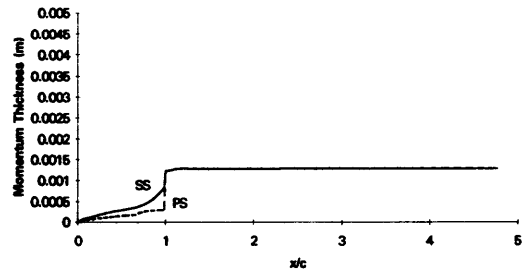
Figure C-2. Stage 67 No Suction.
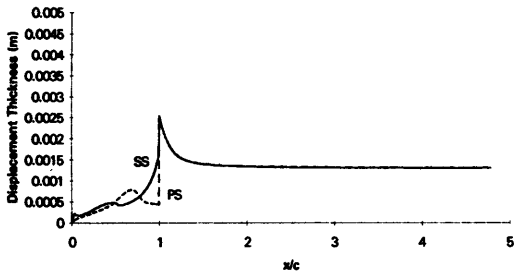
Figure C-3. Stage 67, 25% Suction at 50%c.
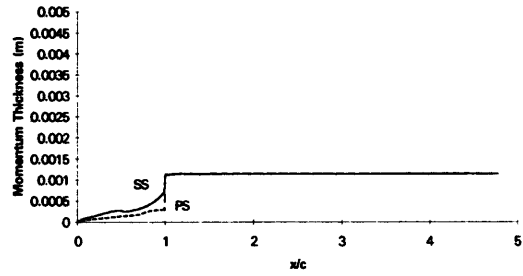
Figure C-4. Stage 67, 25% Suction at 50%c.
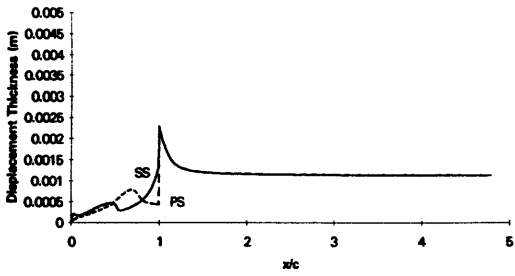
Figure C-5. Stage 67, 50% Suction at 50%c.
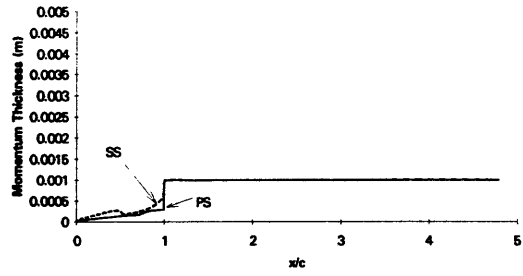
Figure C-6. Stage 67, 50% Suction at 50%c.

77
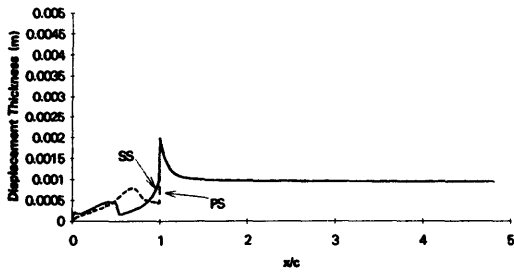
Figure C-7. Stage 67, 75% Suction at 50%c.
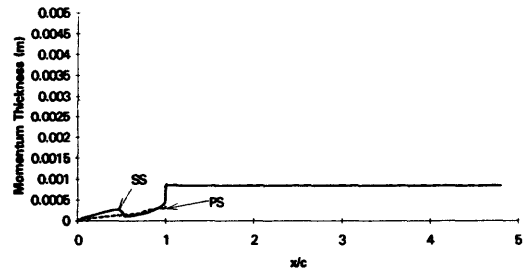
Figure C-8. Stage 67, 75% Suction at 50%c.
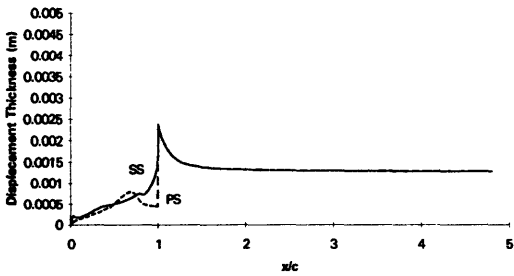
Figure C-9. Stage 67, 25% Suction at 80%c.
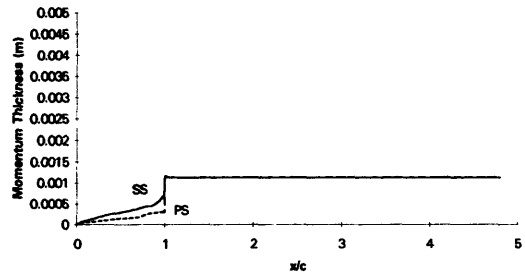
Figure C-10. Stage 67, 25% Suction at 80%c.
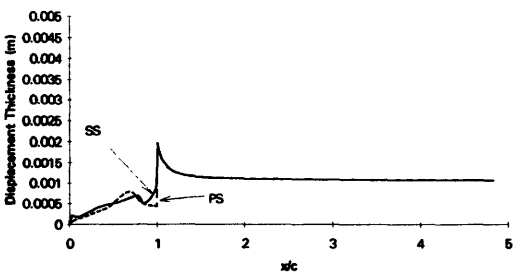
Figure C-11. Stage 67, 50% Suction at 80%c.
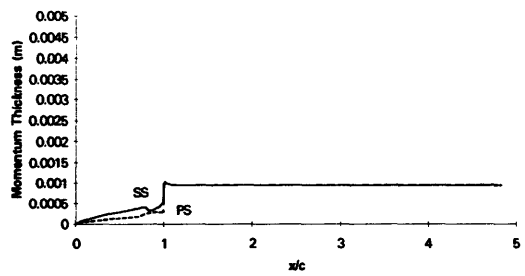
Figure C-12. Stage 67, 50% Suction at 80%c.
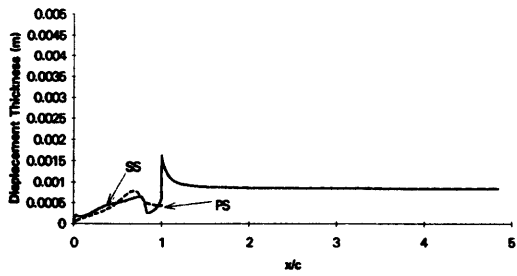
Figure C-13. Stage 67, 75% Suction at 80%c.
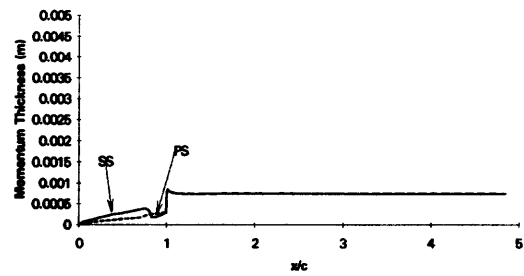
Figure C-14. Stage 67, 75% Suction at 80%c.
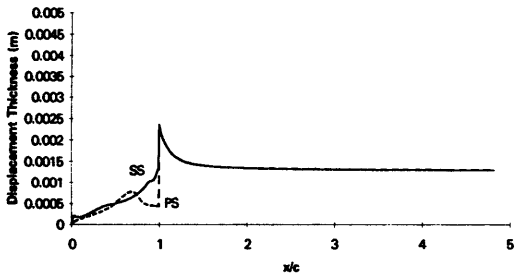
Figure C-15. Stage 67, 25% Suction at 90%c.
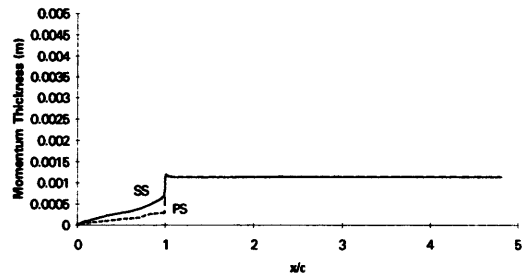
Figure C-16. Stage 67, 25% Suction at 90%c.
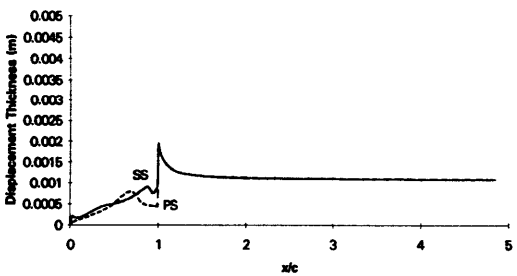
Figure C-17. Stage 67, 50% Suction at 90%c.
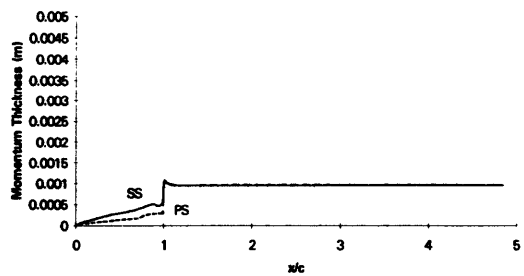
Figure C-18. Stage 67, 50% Suction at 90%c.
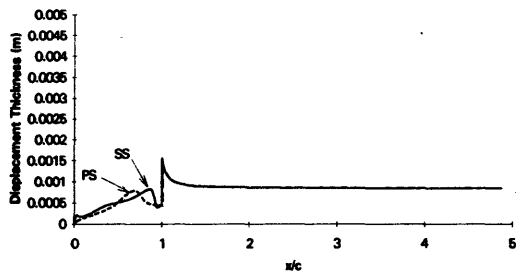
Figure C-19. Stage 67, 75% Suction at 90%c.
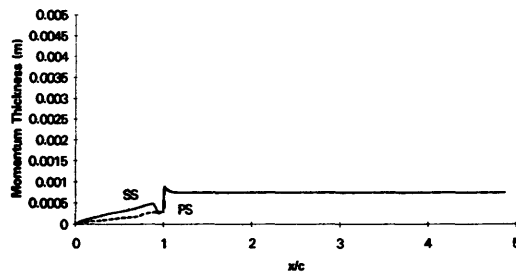
Figure C-20. Stage 67, 75% Suction at 90%c.
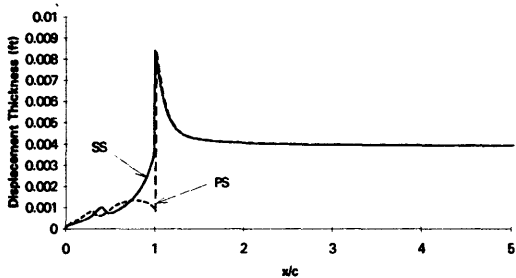
Figure C-21. Test Fan, No Suction.
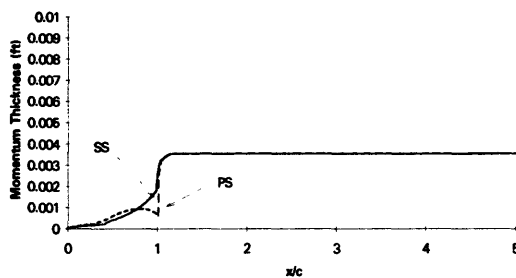

Figure C-22. Test Fan, No Suction.
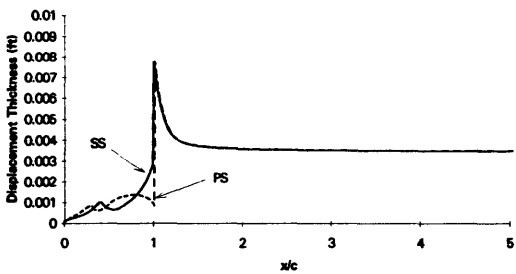
Figure C-23. Test Fan, 25% Suction at 50%c.
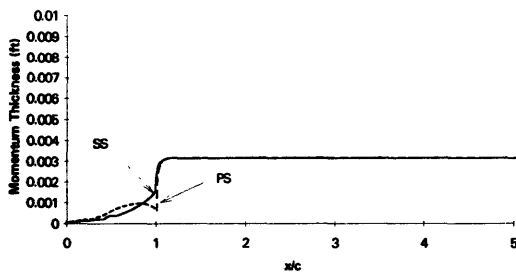
Figure C-24. Test Fan, 25% Suction at 50%c.
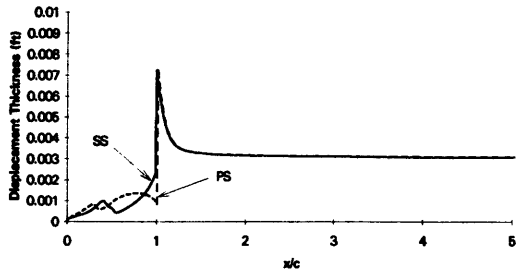
Figure C-25. Test Fan, 50% Suction at 50%c.
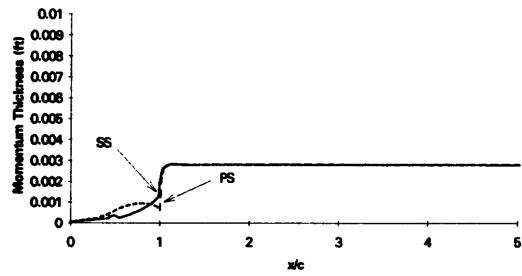
Figure C-26. Test Fan, 50% Suction at 50%c.
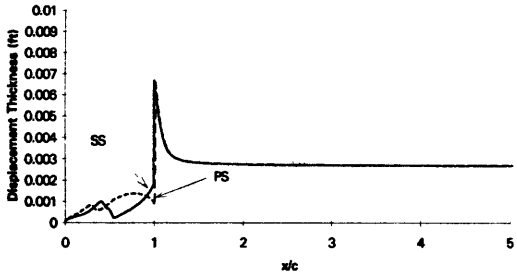
Figure C-27. Test Fan, 75% Suction at 50%c.
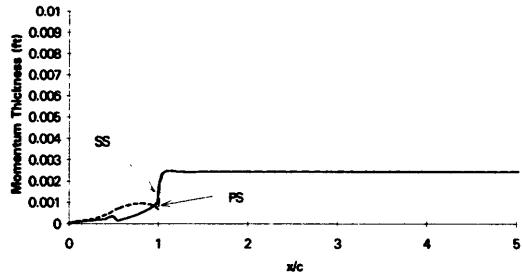
Figure C-28. Test Fan, 75% Suction at 50%c.
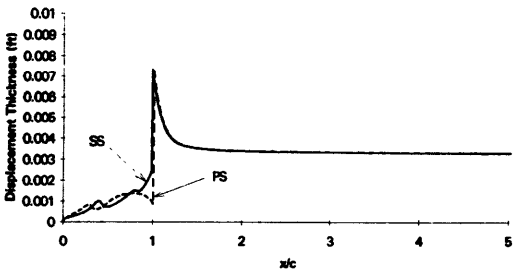
Figure C-29. Test Fan, 25% Suction at 80%c.
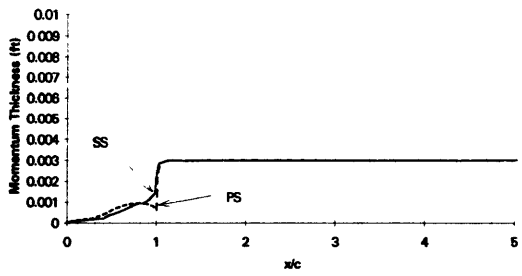
Figure C-30. Test Fan, 25% Suction at 80%c.
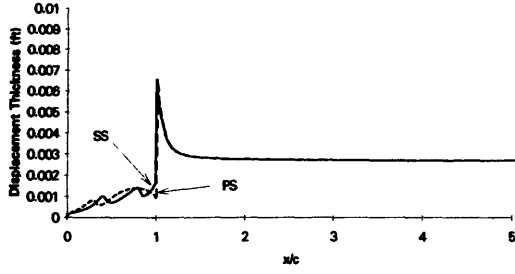
Figure C-31. Test Fan, 50% Suction at 80%c.
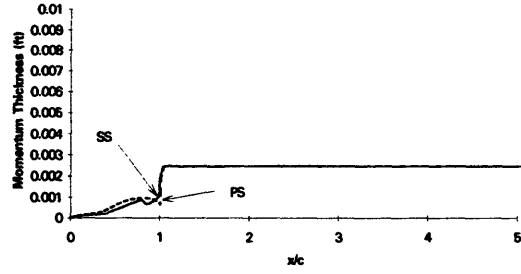
Figure C-32. Test Fan, 50% Suction at 80%c.
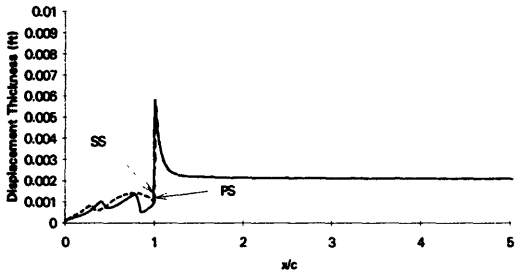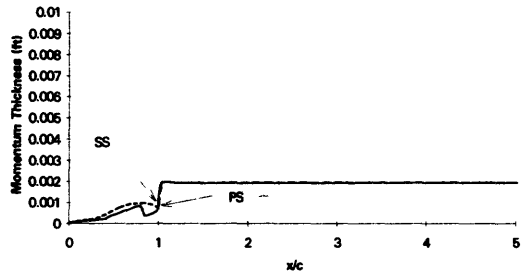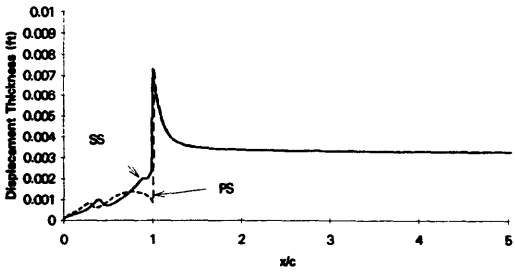

Figure C-33. Test Fan, 75% Suction at 80%c.

Figure C-34. Test Fan, 75% Suction at 80%c.
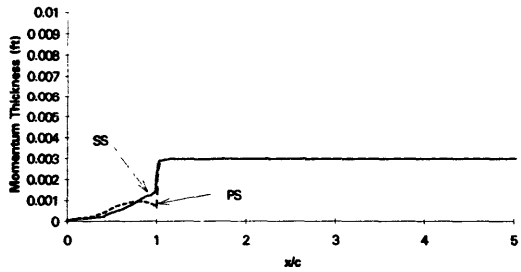

Figure C-35. Test Fan, 25% Suction at 90%c.
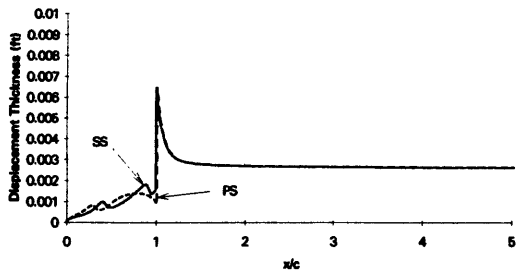

Figure C-36. Test Fan, 25% Suction at 90%c.
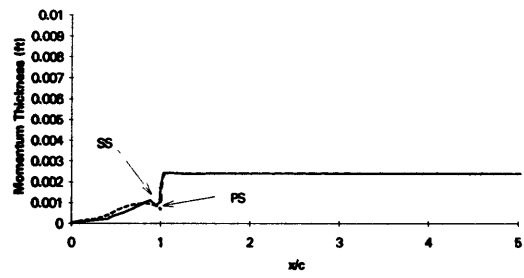
Figure C-37. Test Fan, 50% Suction at 90%c.

Figure C-38. Test Fan, 50% Suction at 90%c.
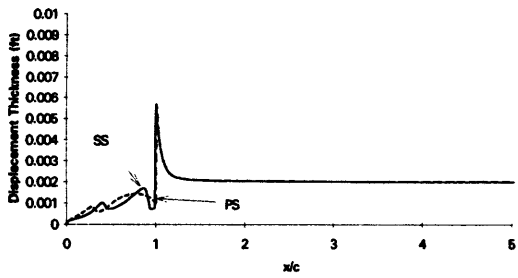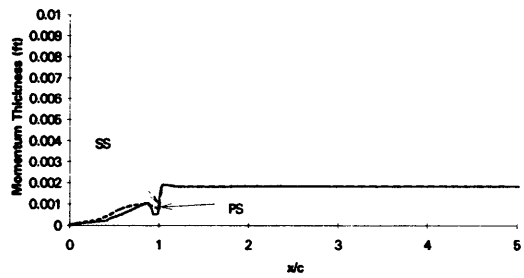

Figure C-39. Test Fan, 75% Suction at 90%c.

Figure C-40. Test Fan, 75% Suction at 90%c.